Aerodynamic and aeroacoustic investigation of vertical axis wind turbines with different number of blades using mid-fidelity and high-fidelity methods

AIAA AVIATION Forum
12-16 June 2023, San Diego, CA and Online
AIAA AVIATION 2023 Forum

10.2514/6.2023-3642

Aerodynamic and aeroacoustic investigation of vertical axis wind turbines with different number of blades using mid-fidelity and high-fidelity methods

Shubham*
Nottingham Trent University, Nottingham, NG1 4FQ, United Kingdom

Nigel Wright†
University of Birmingham, Birmingham, B15 2TT, United Kingdom

Francesco Avallone‡
Politecnico di Torino, Torino, 10129, Italy

Anton Ianakiev§
Nottingham Trent University, Nottingham, NG1 4FQ, United Kingdom

The aerodynamics and aeroacoustics of small-scale Darrieus vertical axis wind turbine (VAWT) are investigated at chord-based Reynolds number below 4×10^5. A statistical temporal and grid convergence study is conducted to analyse the thrust and torque coefficients. Four different VAWTs with different numbers of blades (1, 2, 3, and 4) are investigated using both the high-fidelity Lattice Boltzmann Method (LBM) and mid-fidelity Lifting Line Free Vortex Wake (LLFVW) method. The statistical temporal convergence is achieved much earlier for the 1-bladed rotor than for the 3-bladed rotor, using both methods. Power performance analysis reveals that VAWTs with more blades generate more power at lower Tip Speed Ratios (TSRs), while VAWTs with fewer blades generate more power at higher TSRs. The aerodynamic efficiency of each blade decreases as the number of blades increases, leading to a decreased amplitude of rotor loading variation in a single rotation. Both the mid-fidelity LLFVW and high-fidelity LBM capture these physical trends well. However, LLFVW predicts lower peak C_T and C_Q values in a single rotation and higher streamwise velocities in the wake, as compared to LBM. Moreover, the former predicts higher average power output than the latter, and the discrepancy increases as the number of blades increases. In terms of noise, at constant TSR, low-frequency BPF noise is found to be higher in VAWTs with fewer blades, while high-frequency noise is found to be higher in VAWTs with more blades. Overall Sound Pressure Level values revealed that overall noise increased with an increase in the number of blades except for the 4-bladed VAWT for which the noise decreased.

Keywords

Mid-fidelity, High-fidelity, Lifting Line method, Lattice Boltzmann Method, Vertical Axis Wind Turbine, Aerodynamics, Aeroacoustics, CFD

I. Nomenclature

c = blade chord, m
C_d = airfoil drag coefficient
C_l = airfoil lift coefficient

*PhD researcher, Sustainable Energy Systems, Department of Civil Engineering, shubham.shubham@ntu.ac.uk, AIAA member 1345559
†Professor of Water and Environmental Engineering, Department of Civil Engineering, n.wright.4@bham.ac.uk
‡Professor, Department of Mechanical and Aerospace Engineering, francesco.avallone@polito.it
§Professor, Sustainable Energy Systems, Department of Civil Engineering, anton.ianakiev@ntu.ac.uk

C_T = thrust coefficient
C_Q = torque coefficient
C_P = power coefficient
D = VAWT diameter, m
f = frequency, Hz
h = grid spacing, m
L = blade length, m
M = free-stream Mach number
n = rotations per second, 1/s
Q = VAWT torque, Nm
r = VAWT radius, m
Re = Reynolds number
Re_c = chord-based Reynolds number
T = VAWT thrust, N
u = uncertainty
V_∞ = freestream velocity, m/s
V_{eff} = resultant velocity, m/s
V_{tip} = blade tip velocity, m/s
σ = VAWT solidity
ω = VAWT rotational speed, rad/s
α = angle of attack, $^\circ$
λ = tip speed ratio
ρ = air density, kg/m^3

II. Introduction

The aerodynamics and aeroacoustics of small-scale wind turbines operating at low Reynolds numbers have attracted increasing interest. The focus on sustainability in urban areas has become more significant in recent years, as such areas account for a substantial proportion of a nation's carbon emissions. The United Nations reports that the global urban population is projected to rise by 2.5 billion from 2018 to 2050, which equates to 68% of the world's population residing in urban areas, as opposed to the current 55% [1]. By adopting urban wind turbines as a more sustainable means of energy generation, cities can work towards achieving carbon neutrality. In addition to reducing transmission losses and increasing power generation efficiency [2, 3], localised off-grid systems can raise consumer awareness, thereby enabling them to become energy producers.

The flow conditions in urban areas are turbulent in nature [4]. Consequently, vertical axis wind turbines (VAWTs) have emerged as a more suitable option than horizontal axis wind turbines (HAWTs) due to their superior performance in the urban environment [5]. Furthermore, Dabiri [6] has demonstrated that a VAWT wind farm installed in urban areas can potentially generate an order of magnitude more power per unit area of the ground than a HAWT wind farm located in rural onshore areas. Other advantages of VAWTs include lower cut-in speed and noise levels, omnidirectionality, and ease of maintenance. The most commonly used type of VAWT at present is the Darrieus H-rotor, which comprises straight airfoil-shaped blades that rotate vertically around an axis, generating torque primarily through the lift produced by the blades. Darrieus VAWTs have considerable potential to enhance power generation capacity [7, 8]. However, the rapid growth of the VAWT market will be closely linked to the attenuation of wind turbine rotor noise [9, 10].

VAWTs have a large 3D design space and one of the fundamental design parameters which plays a significant role in determining the aerodynamic and aeroacoustic behaviour is the number of blades. In general, increasing the number of blades of a turbine increases its starting torque, thereby enhancing its performance under low wind speeds. Nevertheless, increasing the blade count also causes a reduction in the overall aerodynamic efficiency of the turbine, primarily because of the presence of blade-wake/blade-vortex interactions and increased drag [11]. Several numerical and experimental investigations have examined the impact of the number of blades on the aerodynamic performance of VAWTs.

Maeda et al. [12] conducted a wind tunnel experiment using a NACA 0021 blade to examine the effect of number of blades on energy performance and aerodynamic forces. The results showed that the power absorbed by the turbine is dependent on the upstream region of the azimuth angle, and the power coefficient decreases with an increase in blade number. A VAWT with two blades provides higher annual generating capacity in high wind velocity areas, while a VAWT with five blades is more suitable for low wind velocity areas. In a separate study, Li et al. [13] used

Laser Doppler Velocimetry (LDV) to measure flow field characteristics and found that the relationship between power coefficient (C_P) and tip speed ratio varies with blade pitch angle, and the maximum C_P differs with blade number. An increase in blade number results in a decrease in the maximum value of C_P and an increase in the maximum value of torque coefficient C_Q. Similar conclusions were reached in another study on the effect of variation in solidity by varying the number of blades [14].

A study by Qu et al. [15] examined the impact of the number of blades on the self-starting performance of a VAWT with self-adapting wind speed (VAWT-SWS), which was compared to a Darrieus straight-bladed wind turbine. The study demonstrated that VAWT-SWS had better self-starting performance than the Darrieus turbine and that an increase in the blade number improved static self-starting performance while degrading dynamic self-starting performance. Sunyoto et al. [16] conducted wind tunnel experiments for an H-Darrieus wind turbine model and concluded that the number of blades affected the rotor rotation, with more blades making it easier for the turbine to rotate at low wind speeds and resulting in shorter performance and higher torque. Howell et al. [17] conducted similar wind tunnel experiments for a 2- and 3-bladed VAWT, and their results support those of Sunyoto.

Delafin et al. [18] employed a vortex model to predict the power coefficient and forces on five different VAWTs with varying numbers of blades (2, 3, and 4). The results indicated that increasing the number of blades while maintaining the same solidity reduced torque, thrust, and lateral force ripples, and a third or fourth blade further reduced these ripples but increased the frequency of maximum loads. Mohamed [19] used numerical simulations to investigate over 20 symmetric and non-symmetric airfoil shapes for VAWTs and found that the S-1046 airfoil improved the power coefficient by 26.83% and efficiency by 10.87% compared to the conventional NACA airfoils. Using S-1046, a low solidity design is recommended for the H-rotor Darrieus turbine to obtain a wider operating range since increasing solidity (by increasing the number of blades) from 0.1 to 0.25 decreased the TSR operating range from 10 to 6. Meanwhile, Sun et al. [20] investigated the effects of fixed offsetting pitching angles and changing blade numbers in VAWTs using the Unsteady Reynolds Average Navier-Stokes (URANS) method. They found that at high wind speeds (> 9 m/s), a turbine with three blades had a larger mean power coefficient than with five blades, and a turbine with more blades and an offsetting pitching angle of -4 degrees had a smaller self-starting period and higher acceleration.

Rezaeiha et al. [21] conducted high-fidelity CFD simulations and found that increasing both solidity and blade number caused the optimal tip speed ratio to shift towards lower values, leading to an increase in the maximum attainable power. The rise in power was attributed to Reynolds number effects, with the increment in power being absent when solidity was increased at a constant Reynolds number. In contrast, Castelli et al. [22] found that increasing the blade number led to reduced efficiency and a lower peak power coefficient, but allowed the maximum power coefficient to be reached at lower angular velocities. Increasing the blade number also led to a decrease in the radial component of the aerodynamic forces, which is desirable from a structural perspective. Similar studies have been conducted by previous researchers regarding the impact of the number of blades [23–32].

Limited studies have been conducted on noise sources in small-scale wind turbines, in contrast to extensive investigations on large-scale Horizontal Axis Wind Turbines (HAWTs). The knowledge gained from the noise studies of HAWTs cannot be applied directly to develop low-noise small-scale VAWTs, mainly because of the differences in aerodynamic phenomena at Reynolds numbers (Re) ranging from 1×10^4 to 1×10^5 for the latter, and differences in fluid dynamic interactions due to the axis of rotation of VAWTs being perpendicular to that of HAWTs. Several studies have reported that VAWTs produce lower noise than HAWTs of similar size and power, which makes them suitable for applications in urban areas [33–35].

The number of blades, or solidity, has a significant impact on the aeroacoustic performance of VAWTs. Higher blade numbers can result in higher noise levels due to increased blade loading, which is a significant concern for their use in urban areas [36]. Exposure to turbine noise has been definitively correlated with annoyance. Understanding the effect of the number of blades on the aeroacoustic signature of VAWTs is therefore crucial for developing low-noise designs.

Mohamed [36] utilised CFD simulations in ANSYS Fluent and Ffowcs Williams and Hawkings (FW-H) methodology to investigate the aerodynamic noise sources associated with VAWTs. The results indicate that a reduction in solidity from 0.25 to 0.1 can decrease noise emissions by 7.6 dB. Additionally, the S-1046 airfoil has been found to be the most optimal due to its minimal aerodynamic noise emissions. Another study by Mohamed [37] examined fifteen different airfoil configurations, including three standard airfoils and twelve J-shaped designs with different cut ratios. The results indicate that the J-shaped design did not contribute to any performance improvement and increased the noise emissions at low frequencies (less than 2500 Hz), as compared to standard airfoils. Increasing solidity led to an increase in noise generated at all frequencies due to an increase in blade drag and pressure fluctuations from the J-shaped design.

Rasekh et al. [38] demonstrated that increasing solidity increases the interference of blades with the wake region, reducing the effective angle of attack and increasing steady loading noise at blade passage frequency (BPF). Averaged

Overall Sound Pressure Level (OSPL) values (calculated by averaging the value of OSPL at different azimuthal positions) increase as solidity decreases. Various other authors have worked on characterising the VAWT noise generated using numerical and experimental methods [39–43].

Despite the available literature, there is still a lack of comprehensive studies using full 3D high-fidelity numerical simulations on the flow physics of unsteady blade loads and downstream turbulent near-wake of VAWTs. Furthermore, the capability of mid-fidelity analytical aerodynamic methods to capture the effects of blade number on VAWT force and flow field is not well understood. In aeroacoustics, there is a research gap in identifying the impact of blade number on VAWT aeroacoustic performance and noise sources. Therefore, this study aims to take the first step towards creating a multi-fidelity simulation framework. This is achieved by conducting high-fidelity 3D aerodynamic simulations using Lattice Boltzmann Method (LBM) and mid-fidelity simulations using the Lifting Line Free Vortex Wake (LLFVW) method for straight-bladed VAWTs. Aeroacoustic post-processing is performed using the Ffowcs Williams and Hawkings (FW-H) methodology to calculate the far-field noise.

The objective is to gain insights into the different fluid dynamic interactions for different number of blades that can be captured by both methods. High-fidelity simulations enable accurate resolution of flow around VAWT blades and downstream wake to study 3D effects on force and flow field, including non-uniform blade loading and non-uniform wake, dynamic stall, blade-vortex interaction, and wake recovery. On the other hand, the mid-fidelity simulation offers simplified modelling of the flow field using vortex lifting lines and aids in a fundamental understanding of the 3D effects for different blade numbers. A comparative analysis between the two methods can determine the potential of the mid-fidelity method as a substitute for high-fidelity simulation to save significant time and computational resources.

The paper is structured as follows. Section III presents the computational methodology used in QBlade and PowerFLOW, and a description of the geometry and setup. Section IV presents the results obtained for Darrieus VAWTs using both mid-fidelity LLFVW and high-fidelity LBM methods for different number of blades. Finally, section V outlines the conclusion for the present study and recommendations for future studies.

III. Methodology and Setup

A. Numerical computations

1. Flow solver - QBlade

The lifting line method belongs to a family of various "vortex methods", the computational cost of which falls somewhere in between low-fidelity momentum methods (BEMT, DMS, etc.) and high-fidelity CFD methods (Navier Stokes, Lattice-Boltzmann). In the present study, the lifting line theory coupled to a free vortex wake model is used to calculate the VAWT three-dimensional (3D) unsteady flow field past the rotor and the interaction between blade and fluid flow [44, 45]. The LLFVW algorithm is based on nonlinear lifting line formulation by Garrel [46] and is mentioned in detail by Balduzzi [45].

The fluid is modelled as incompressible, inviscid and irrotational; the blade is modelled with a single line of vortices which is located on the quarter chord points of the blade. The wake is discretised into vortex line elements (straight or curved) and these elements are shed at the blade trailing edges at every time step. They then undergo free convection past the rotor ("free wake method") in which the position of the wake end nodes is updated based on the local velocity, which is a combination of inflow velocity and induced velocity from all the wake elements in the domain. Nonlinear in the "nonlinear lifting line formulation" means the circulation calculated on the lifting line bound vortices is acquired from the nonlinear airfoil lift and drag data provided as input. Lift and drag forces are then calculated based on the local angle of attack (α).

The vortex elements are desingularised using the van Garrel's cut-off method [47] with the vortex core size, taking into account viscous diffusion via the vortex core size that is modelled through the kinematic viscosity ν, a turbulent vortex viscosity coefficient δ_ν, and a time offset parameter S_c using the below equation:

$$r_c = \left(\frac{5.03 \delta_\nu \nu \, (t + S_c)}{1 + \varepsilon} \right)^{1/2} \tag{1}$$

The effects of unsteady aerodynamics and dynamic stall are introduced via the ATEFlap aerodynamic model [48, 49] that reconstructs lift and drag hysteresis curves from a decomposition of the lift polars. The implemented ATEFlap formulation has been further adapted to work under the complex conditions of VAWT exhibiting large fluctuations in the angle of attack when rotating at low TSR [50]. Wake reduction schemes have been implemented to lower computational

requirements [48–51]. In the present study, all results with this method will henceforth be referred to with the 'LLFVW' nomenclature.

2. Flow solver - PowerFLOW

The Lattice Boltzmann Method (LBM) is used to compute the flow field because it was shown to be accurate and efficient for similar low Reynolds number rotor applications [52] [53]. The commercial software 3DS Simulia PowerFLOW has been already validated for aerodynamic and aeroacoustic studies on rotors in general [54–56]. The software solves the discrete Lattice Boltzmann (LB) equation for a finite number of directions. For a detailed description of the method, the reader can refer to Succi [57] and Shan et al. [58], while to Chen and Doolen [59] for a review. The LB method determines the macroscopic flow variables starting from the mesoscopic kinetic equation, i.e. the LB equation. The discretization used for this particular application consists of 19 discrete velocities in three dimensions (D3Q19), involving a third-order truncation of the Chapman-Enskog expansion [60]. The distribution of particles is solved by means of the LB equation on a Cartesian mesh, known as a lattice. An explicit time integration and a collision model are used. For the collision term, the formulation based on a unique Galilean invariant [61] is used. The equilibrium distribution of Maxwell-Boltzmann is adopted [60].

To take into account the effect of the sub-grid unresolved scales of turbulence, a Very Large Eddy Simulation (VLES) model is implemented. Following Yakhot and Orszag [62], a two-equations $k-\epsilon$ Renormalization Group is used to compute a turbulent relaxation time that is added to the viscous relaxation time. To reduce the computational cost, a pressure-gradient-extended wall-model is used to approximate the no-slip boundary condition on solid walls [63, 64]. The model is based on the extension of the generalised law-of-the-wall model [65] to take into account the effect of pressure gradient. These equations are iteratively solved from the first cell close to the wall in order to specify the boundary conditions of the turbulence model. For this purpose, a slip algorithm [59], obtained as generalization of a bounce-back and specular reflection process, is used.

Far-field noise is computed using the Ffowcs Williams and Hawkings [66] (FW-H) acoustic analogy. In particular, the formulation 1A of Farassat and Succi [67] extended to a convective wave equation is used in this study [68]. The formulation has been implemented in the time domain using a source-time dominant algorithm [69]. Pressure fluctuations are recorded on three permeable surfaces enclosing the wind turbine and its wake. These pressure fluctuations are used as input to the FW-H solver, thereby including all noise sources inside the three surfaces. Pressure fluctuations are also captured on all solid surfaces (blade surfaces), which when input to the FW-H solver will include noise sources only on the solid surfaces.

3. Wind turbine geometry

A straight-bladed vertical axis wind turbine (VAWT) design with geometrical parameters that are replicated from Balduzzi et al. [45] is utilised. The results obtained by Balduzzi et al. are employed to validate a single-bladed rotor. To investigate flow physics, four different configurations are simulated with varying numbers of blades (1, 2, 3, and 4). An example of the geometric model for the 2-bladed and 4-bladed rotors is shown in Figure 1, while Table 1 presents the geometric values and operational conditions for all configurations. The VAWT solidity is set at 0.08 for the single-bladed rotor and increases proportionally with the number of blades. The rotor aspect ratio for all configurations is 1.46. The inclusion of additional blades (i.e., higher solidity) results in stronger three-dimensional (3D) effects and increased blade-vortex interaction. These fluid dynamic interactions are expected to lead to differences in the unsteadiness of VAWT blade loading, which, in turn, affects wake dynamics and aeroacoustic behaviour.

Table 1 VAWT geometry and operational settings

	Blade length (L)	**Rotor diameter (D)**	**Chord length (c)**	**Freestream velocity (V_∞)**	**Airfoil**
VAWT benchmark [45]	1.5 m	1.03 m	0.086 m	9 m/s	NACA 0021

The current study involves high-fidelity LBM to simulate all the VAWT configurations. Each configuration is also simulated using the mid-fidelity LLFVW method. Obtaining accurate and high-quality airfoil data is vital to produce precise results through low and mid-fidelity methods. To achieve this objective, a virtual geometry is derived from the NACA 0021 profile to account for the virtual camber effect [70]. This process is accomplished through the conformal transformation technique based on the chord-to-radius ratio, as described by Bianchini et al. [71]. The transformed

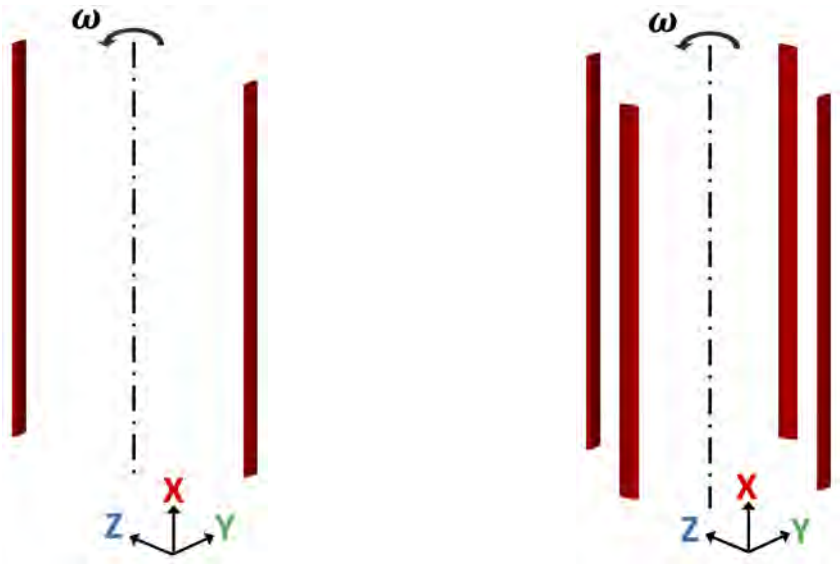

(a) 2-bladed (b) 4-bladed

Fig. 1 VAWT configuration used in this chapter (Balduzzi [45])

airfoil is presented in Figure 2 (a). Lift and drag polars are obtained for Reynolds numbers ranging between 1×10^5 and 1×10^6 using XFoil [72]. This process employs an *NCrit* value of nine and forced transition at the leading edge of both the pressure and suction side. The airfoil static polar data is extrapolated to 360° angle of attack (AoA) using the Montgomerie method [73] to ensure a smooth extrapolation in the post-stall regime. An example of the 360° extrapolated polars is presented by Balduzzi et al. [45].

4. Numerical setup

A simulation volume is implemented, which is a cube with each side measuring $100D$, with the Darrieus geometry positioned at the centre of the volume. The boundary conditions are presented in Figure 2 (b). The velocity inlet is set to the freestream velocity V_∞ in the direction of the Y-axis. An ambient pressure of 101.325 kPa is applied at the pressure outlet. The blade surface is subjected to a no-slip boundary condition. PowerFLOW generates a Cartesian volume grid around the individual solid components in the domain by beginning with the minimum hexahedral cell (voxel) size and a specified number of variable resolution (VR) levels. The VR levels are arranged in a range from fine to coarse, with a voxel size change factor of 2 between adjacent VRs which creates distinct VR regions. The software automatically intersects the Cartesian mesh with the solid parts to produce a collection of polygons, or surfels, that represent the true surface of the body. To optimise computational efficiency, the present study utilises 17 VR regions, with higher resolutions near the blade surface with an offset, and coarser regions located farther from the blade and rotor. This methodology permits the allocation of computational effort primarily to areas of interest and where high flow gradients are anticipated.

Figure 2 (b) presents three red spherical surfaces enclosing the rotor flow field, which function as FW-H permeable surfaces to eliminate hydrodynamic fluctuations in the VAWT wake vortices. The averaging of pressure data obtained from all the permeable surfaces assists in reducing spurious noise sources. The blade surfaces of the VAWT are identified as FW-H solid surfaces. Although the use of the FW-H permeable formulation is a possible alternative, it has not been utilised in this study since it is difficult to eliminate spurious noise sources from FW-H permeable data using only three spherical surfaces in the context of a VAWT. In future studies, a separate investigation will examine the implementation of the FW-H permeable formulation for VAWT aeroacoustics in a more efficient manner. To ensure accurate acoustic wave capture, a criterion of a minimum of 15 points per wavelength is selected, and pressure data are sampled at 8000 Hz for 8 complete rotor rotations. Subsequently, noise spectra are calculated using a Hanning window with 50% overlap and a frequency resolution (Δf) of 15 Hz.

For the LLFVW simulation, Table 2 outlines the values of the simulation parameters utilised.

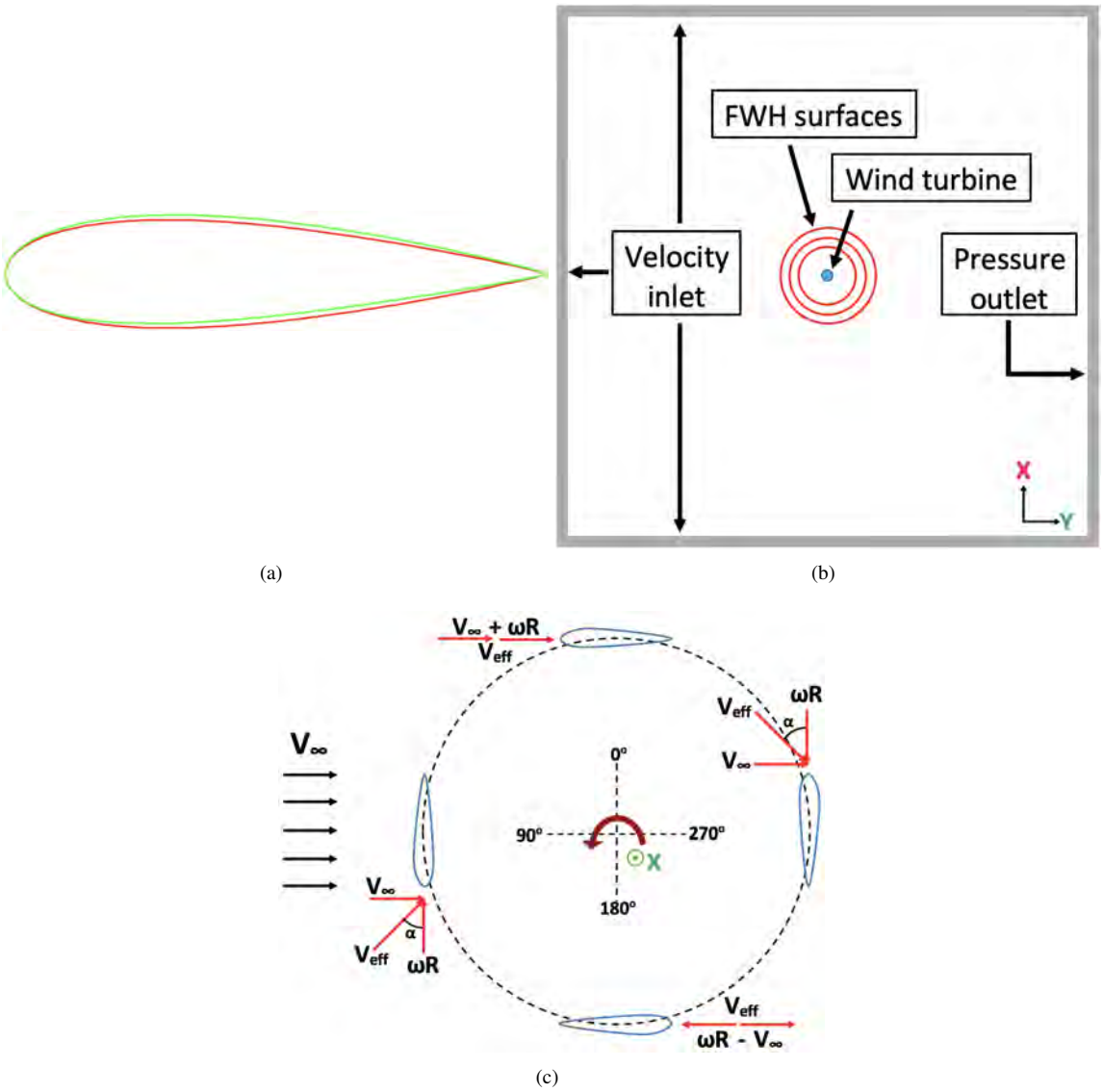

Fig. 2 Numerical setup (a) Virtual camber airfoil (green) and original airfoil (red) for low-fidelity simulation (b) Schematic representation of the simulation domain (c) Position of Darrieus blades over a single rotation, along with velocity diagram in the blade reference frame (adapted from Shubham [74])

5. Flow conditions and grid settings

For the present study, the operational setting of the VAWT for the high-fidelity method (LBM) is depicted in Table 3, using the tip speed ratio (TSR) as a measure of the system's operational condition. TSR is defined as the ratio of the blade rotational speed and the freestream velocity, where ω, r, and V_∞ denote the rotational speed in radians per second, the wind turbine radius, and the freestream velocity, respectively. The freestream velocity is kept constant at 9 m/s, which corresponds to the reference value [45], while ω is adjusted to vary the TSR value. This approach mimics real-life situations, where the rotational speed is adapted based on wind speed measurements to maintain the TSR close to its optimal value. The freestream Mach number (M) is 0.026, and the chord-based Reynolds number (Re_c) is 1.73×10^5. The high-fidelity method (LBM) is exclusively utilised for TSR = 3.3, while the mid-fidelity method (LLFVW) is employed to simulate a range of TSR from 1 to 7. It is important to note that all operational conditions considered in this study have Re_c below 4×10^5. The values of freestream turbulence intensity (I_t) and turbulence length scale (L_t) are set to 0.1% and 1 mm, respectively. However, it is anticipated, based on a prior study [55], that these parameters will

Table 2 Simulation parameters used for the LLFVW method

	LLFVW
Freestream velocity V_∞	9 m/s
Density	1.225 kg/m^3
Kinematic viscosity	1.65 e-5 m^2/s
Blade discretization	31 (cosine)
Azimuthal discretization	3 deg
Full wake length	12
Vortex time offset	1 e-4 sec
Turbulent vortex viscosity	100

not significantly influence the evolution of the unsteady flow field.

Table 3 VAWT operational settings for the high-fidelity method (LBM)

Parameter	**Value**
Tip speed ratio (TSR)	3.3
Rotations per minute (RPM)	550.71
Chord-based Reynolds number (Re_c)	1.73×10^5

In the context of the grid convergence study, the high-fidelity LBM is used to simulate each TSR at four different grid resolutions. The variable resolution (VR) regions near the blade surface have different voxel densities per chord for 'Grid 1', 'Grid 2', 'Grid 3', and 'Grid 4', with the minimum and maximum voxel densities allocated to 'Grid 1' and 'Grid 4', respectively. The resolutions of other VR regions are adjusted proportionally. Table 4 presents the y+ values and voxels per chord for all the grid resolutions. The y+ value is a dimensionless parameter which represents the distance of the first cell centre from the computational domain's wall in the wall-normal direction and is calculated using the average velocity value experienced by the blade at the mid-span location over a single rotation. The voxels per chord indicate the number of grid cells along the blade chord direction.

The voxel sizes for 'Grid 1' and 'Grid 4' are 0.964 mm and 0.321 mm, respectively. For the 2-bladed VAWT, the fine equivalent voxels in the computational domain are 5.3 million and 45.4 million for 'Grid 1' and 'Grid 4', respectively. These fine equivalent voxels are obtained by multiplying the number of voxels by the time stepping rate, which is directly proportional to the mesh resolution level. It is important to note that doubling the voxel size results reduces the computational cost to half, as the time step also doubles. The CPU hours required for simulating 12 rotor rotations (1.31 s) using 'Grid 1' and 'Grid 4' for the 2-bladed VAWT are 2613 and 44720, respectively. These simulations are conducted using a Linux workstation equipped with an AMD Ryzen Threadripper 3990X Gen3 64 Core 128GB DDR4 3GHz platform. Both the fine equivalent voxels and CPU hours scale proportionally with the number of blades for different VAWT configurations. The physical time step for 'Grid 1' and 'Grid 4' corresponds to a Courant-Friedrichs-Lewy (CFL) number of 1 in the finest VR level and is 4.53×10^{-6} s and 1.51×10^{-6} s, respectively.

Table 4 VAWT grid settings for the high-fidelity LBM simulation

		Grid 1	**Grid 2**	**Grid 3**	**Grid 4**
VAWT benchmark [45]	y+	100	62.5	50	33.3
	Voxels per chord	8.9×10^1	1.42×10^2	1.78×10^2	2.67×10^2

The integral and time-varying behaviour of the VAWT thrust coefficient (C_T) and torque coefficient (C_Q) are reported and grid convergence parameters are analysed for all the above-mentioned cases. These coefficients are defined as:

$$C_T = \frac{T}{0.5\rho A V_\infty^2} \tag{2}$$

$$C_Q = \frac{Q}{0.5\rho A V_\infty^2 r} \tag{3}$$

where, T and Q are VAWT thrust and torque respectively, ρ is the air density, A is swept area ($D \times L$) where is D is rotor diameter and L is blade length, R is rotor radius and V is freestream velocity. Using high-fidelity LBM, Sound Pressure Level (SPL) spectra and Overall SPL (OSPL) values are also reported and analysed.

IV. Results

A. Grid convergence study and validation

Figure 3 depicts the temporal convergence characteristics of the thrust coefficient (C_T) and torque coefficient (C_Q) for two distinct VAWT configurations, namely the 1-bladed and 3-bladed rotor, as obtained using high-fidelity LBM (for the finest Grid 4) and mid-fidelity LLFVW method. The reported values in the figures are representative of the overall rotor, comprising all blades in a rotor. The corresponding uncertainty values (u) are calculated as a percentage of the standard deviation of thrust and torque values averaged over a complete rotation. These uncertainty values reflect the degree of uncertainty or variability in the computed thrust and torque coefficients over time due to the inherent unsteadiness and randomness in the fluid dynamic interactions. A smaller value of u implies a higher level of confidence in the simulation outcomes, indicating that the simulation has achieved temporal convergence. All u values depicted in the figures are calculated after the 10th rotor rotation for LBM and the 20th rotor rotation for LLFVW.

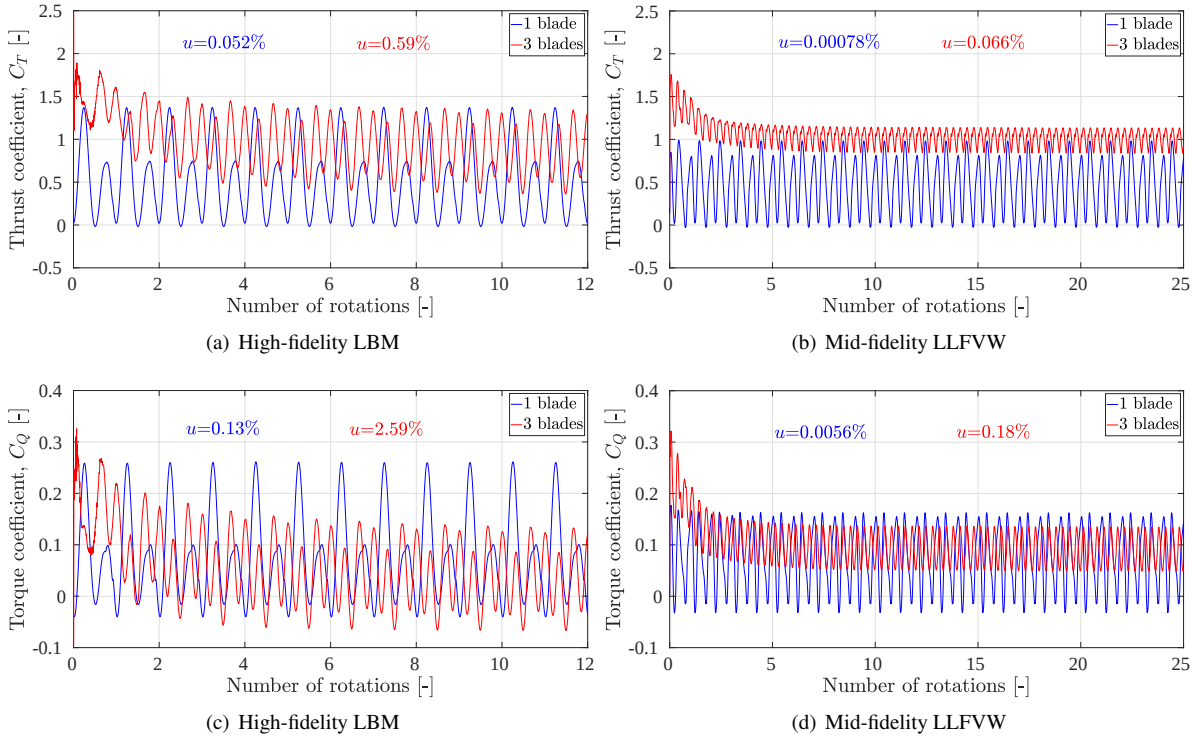

(a) High-fidelity LBM (b) Mid-fidelity LLFVW

(c) High-fidelity LBM (d) Mid-fidelity LLFVW

Fig. 3 Statistical temporal convergence study for VAWT thrust coefficient C_T and torque coefficient C_Q using the high-fidelity LBM and mid-fidelity LLFVW, for the finest Grid 4

It is observed from the figures that the statistical temporal convergence is attained much earlier for the 1-bladed rotor than for the 3-bladed rotor, using both LBM and LLFVW methods. Specifically, convergence is reached after

approximately 4 rotations for LBM and 6 rotations for LLFVW in the case of the 1-bladed rotor, while it takes around 8 rotations for LBM and 10 rotations for LLFVW for the 3-bladed rotor. The low values of uncertainty (u) for both configurations confirm the temporal convergence. Notably, the mid-fidelity LLFVW method is capable of accurately capturing this unsteady phenomenon in a VAWT force field, as evidenced by the convergence results. Interestingly, these outcomes are contrary to those reported by Rezaeiha [75], wherein more than 20 rotations were necessary to attain temporal convergence in a high-fidelity CFD simulation. It is pertinent to mention that in this study, the LBM simulations for the finer grid are initiated using the results from the coarser grid, which may have contributed to the reduced transient period. This seeding approach conforms to the current best practice for simulations of this type, where a coarser resolution is simulated first for a minimum of 10 rotor rotations. The final frame of this simulation is then used to seed a finer resolution simulation, which is executed with an initial settling time of a few blade-passage periods [55].

Similarly, Figure 4 illustrates the temporal convergence of unsteady pressure data acquired using the high-fidelity LBM for the finest Grid 4. The data is collected at a specific location in the blade mid-span plane of rotation, situated at a distance of $7D$ from the VAWT centre, in the lateral direction (0,0,$7D$). To conserve computational resources, the pressure data is recorded starting from the 6th rotation. It can be observed that temporal convergence is achieved after the 6th rotation for both 2-bladed and 4-bladed rotors. In this study, all subsequent results are reported on data obtained after the 10th rotation for the high-fidelity LBM and the 20th rotation for the mid-fidelity LLFVW.

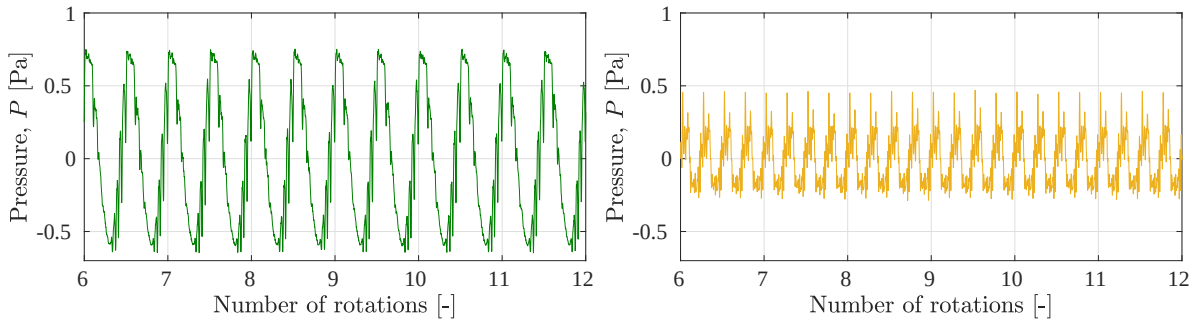

(a) 2-bladed (b) 4-bladed

Fig. 4 Statistical temporal convergence study for unsteady pressure data at TSR = 3.3 at location (X,Y,Z)=(0,0,7D), using the high-fidelity LBM for the finest Grid 4

Two VAWT configurations, a 1-bladed and a 2-bladed rotor, are studied using the four different grids. The results of the grid convergence study for the overall rotor's thrust coefficient (C_T) and torque coefficient (C_Q) are depicted in Figure 5. This type of study is crucial to verify the independence of the results from the numerical grid employed. The grid resolution is expressed as the grid spacing h, normalised with respect to the blade chord c, where h corresponds to the smallest grid size in the numerical domain. Furthermore, the figure shows the values obtained using the Richardson extrapolation method [76], which can be used to calculate C_T and C_Q when $h/c \rightarrow 0$, indicating the approach towards the continuum limit or utilizing an infinite number of cells in the Cartesian grid. Each figure also displays the grid convergence index (GCI), calculated based on the difference between two adjacent grid resolutions, providing an estimate of the solution error [76, 77].

The results of the grid convergence study reveal that the thrust values show better grid convergence than the torque values for both configurations. The 2-bladed rotor demonstrates the lowest GCI for thrust values between Grid 3 and Grid 4. These findings suggest that a coarser grid can suffice to obtain converged blade loading values, while a finer grid is required for converged blade torque or power values. This is due to the strong dependency of blade skin friction and drag values on the variation in y+ values. Accurate prediction of airfoil drag for both low and high Reynolds number flows is still an area of active research [78]. GCI_{34} is consistently lower than GCI_{23} for all cases, indicating that increasing the grid resolution may result in more accurate and reliable results for the VAWT setup presented in this study, as the difference related to the numerical grid decreases with higher resolution. However, it is worth noting that this is not always the case with VAWT simulations, and the relative GCI values can vary depending on the simulated tip speed ratio and rotor scale [76]. Furthermore, a previous investigation by Shubham et al. [76] revealed that the grid convergence of Overall Sound Pressure Level (OSPL) was found to be comparable to that of thrust values and better than torque values. As a result, Grid 4 is deemed to be converged for both aerodynamics and aeroacoustics and is therefore selected for all future numerical simulations. It is considered sufficient to provide an accurate physical analysis

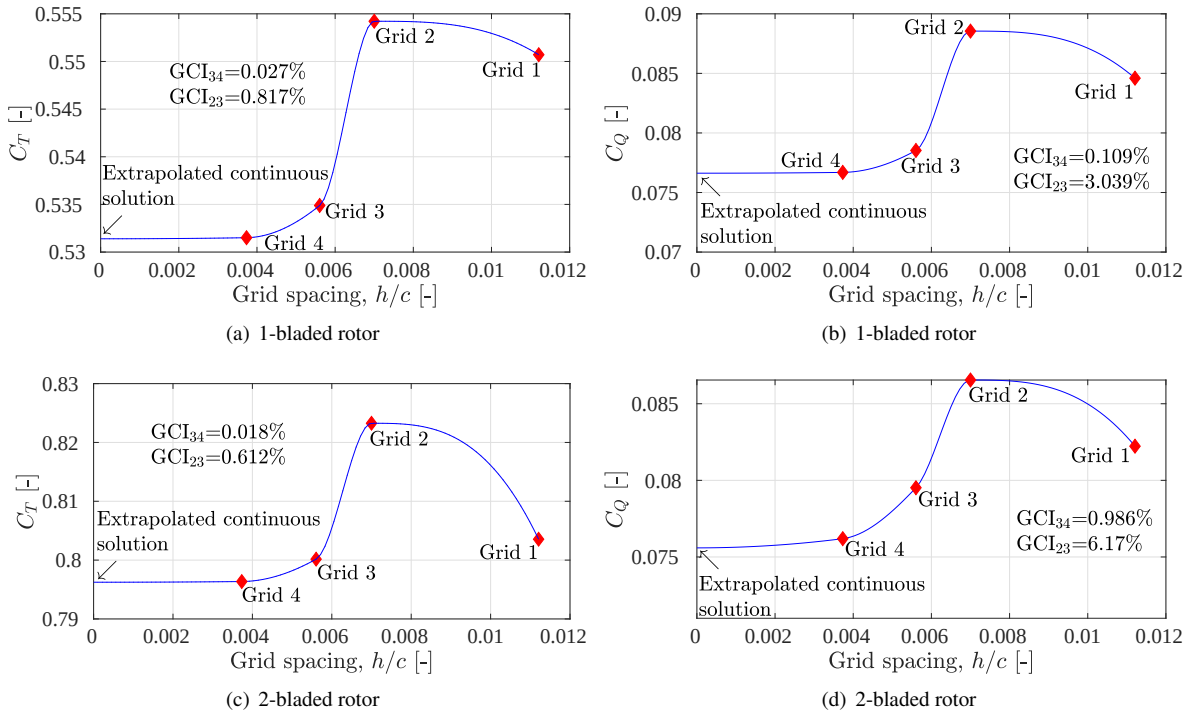

Fig. 5 Grid convergence study for VAWT thrust coefficient C_T and torque coefficient C_Q using the high-fidelity LBM

of VAWT fluid dynamic interactions.

Figure 6 depicts a comparison of the power coefficient (C_P) values for the 1-bladed VAWT obtained from the mid-fidelity and high-fidelity methods of the current study with the reference dataset reported by Balduzzi et al. [45]. The reference dataset consists of the mid-fidelity LLFVW method and the high-fidelity 3D CFD method, utilizing the compressible formulation of the Reynolds-averaged Navier-Stokes (RANS) equations, only for a TSR of 3.3. The LLFVW method predicts the typical VAWT power curve shape [79, 80] over the entire TSR range, exhibiting a close agreement with the reference data. The C_P value obtained at TSR = 3.3, using the high-fidelity LBM method corresponding to Grid 4, closely matches all three other results. The validation of both numerical setups in the current study is deemed to be excellent, not only with the published data but also between each other. Hence, they can be utilised to further investigate VAWT fluid dynamic interactions and wake dynamics. The next sections will compare the mid-fidelity and high-fidelity results for different numbers of blades, highlighting the effects of differences in numerical modelling as the VAWT geometry changes, and aeroacoustic results.

B. Aerodynamics

Fig. 7 displays the power coefficient (C_P) and thrust coefficient (C_T) values obtained for the four VAWT configurations with 1, 2, 3, and 4 blades. The mid-fidelity LLFVW is simulated for the entire range of TSR, while high-fidelity LBM is simulated solely for TSR = 3.3. It is expected that high-fidelity simulations at TSR of 3.3, complemented by mid-fidelity simulations encompassing a range of TSR values, will yield substantial insights into the fluid dynamic interactions of a VAWT when the number of blades is varied.

The mid-fidelity results indicate several trends. At lower TSRs, more blades generate more power, while the opposite is true at higher TSRs. At low TSR, blades act more independently and increasing solidity has little effect on blade-wake/blade-vortex interaction, resulting in increased total blade tangential loading and power production. As TSR increases, induction factor and blade-wake/blade-vortex interaction also increase, and increasing solidity worsens tangential loading on each blade and overall rotor power. As a result, higher solidity produces a sharper gradient in C_P values than lower solidity cases over the entire range of TSR. These findings suggest that VAWT design optimization aimed at improving its self-starting capability (C_P at very low TSR) would benefit from higher solidity

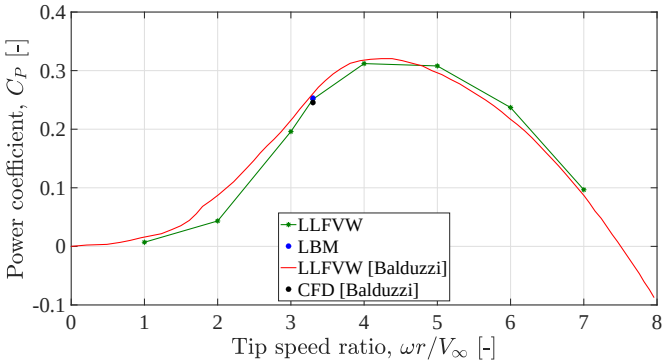

Fig. 6 C_P values for a 1-bladed VAWT obtained using mid-fidelity LLFVW and high-fidelity LBM compared with the results reported by Balduzzi et al. [45]

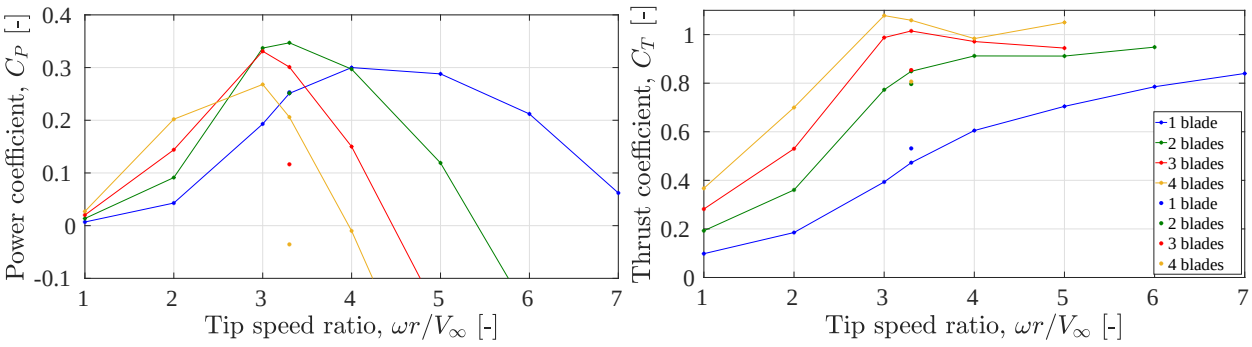

(a) Power coefficient, C_P (b) Thrust coefficient, C_T

Fig. 7 Power and thrust curve obtained for different number of blades using the mid-fidelity LLFVW and high-fidelity LBM; line plot is for mid-fidelity LLFVW and single dot at TSR = 3.3 is for high-fidelity LBM

designs. Similarly, C_P values show that optimal TSR decreases as the number of blades increases. These observations are a well-established norm for a VAWT [5] and are reasonably modelled by the mid-fidelity approach. The thrust coefficient (C_T) shows a positive trend with both an increase in TSR and the number of blades. Above TSR = 3, VAWT with a higher number of blades exhibits an asymptotic trend, with the values starting to decrease for 3- and 4-bladed rotors as TSR increases.

At TSR of 3.3, the difference between C_P values obtained using LBM and LLFVW increases with an increase in the number of blades. LBM predicts lower C_P values compared to LLFVW, except for the 1-bladed rotor where the match is very good. The difference in C_P values is small (0.0021) for the 1-bladed rotor, while it increases to 0.11, 0.15, and 0.25 for the 2, 3, and 4-bladed rotors, respectively. In the LBM case, the power generation becomes negative for the 4-bladed rotor. A similar trend is observed for the thrust coefficient (C_T) values, where the difference between the two methods increases with the number of blades. These observations suggest that the LLFVW method may not be able to capture the complex 3D effects in the flow and force fields in a VAWT as strongly as LBM, especially when the number of blades increases. This is particularly true in the near-wake region where blade-wake and blade-vortex interactions are significant. This discrepancy is not unexpected, given the inherent differences in fluid modelling between the two methods. For the same reason, the asymptotic or decreasing trend in C_T values obtained using LLFVW for higher TSRs is shown by LBM results even at a lower TSR of 3.3, where the 4-bladed rotor produces lower thrust than the 3-bladed rotor. An investigation with even more blades can provide further insights into the effect of the number of blades on C_T variation.

Figure 8 displays the variation in C_T and C_Q for the overall rotor over a 360° azimuth angle at TSR = 3.3, as obtained from high-fidelity LBM and mid-fidelity LLFVW methods. The figure also presents the average values over a complete rotation which corresponds to the values shown in Figure 7. The investigation highlights that as the number of blades

increases, the amplitude of variation in thrust and torque values over the azimuth angle reduces, resulting in a smoother overall rotor loading variation. This is due to the distribution of the rotor loading over more blades as the number of blades increases. Specifically, at any instant, the peak loading of one blade in the upwind part of the rotation is balanced by a reduced loading of another blade in the downwind part of the rotation.

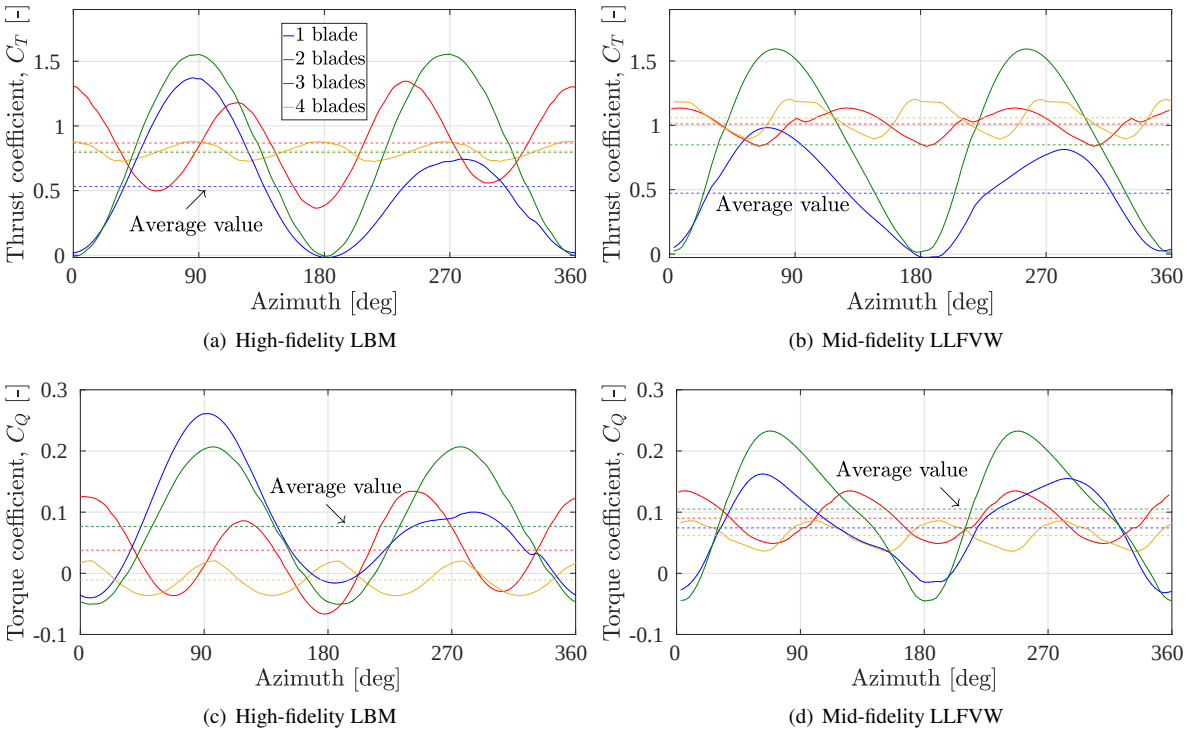

(a) High-fidelity LBM (b) Mid-fidelity LLFVW

(c) High-fidelity LBM (d) Mid-fidelity LLFVW

Fig. 8 Variation of thrust coefficient C_T and torque coefficient C_Q for the overall rotor over a complete rotation, using the high-fidelity LBM and mid-fidelity LLFVW at TSR = 3.3

The mid-fidelity LLFVW and high-fidelity LBM both model this physical behaviour well. However, when comparing the peak C_T and C_Q values in the upwind and downwind parts of the rotation, LLFVW predicts lower values as compared to LBM, except for the 2-bladed rotor where there is a good agreement. This trend can also be observed in the statistical time convergence results shown in Figure 3. The cause of this trend is attributed to the XFOIL polar values (C_l and C_d vs angle of attack α) used in the analytical formulation of LLFVW, which influence the blade angle of attack and induced velocity. These results suggest the need to modify the polars accordingly by incorporating empirical corrections in future studies. Alternatively, the airfoil polar values for 360° AoA obtained from wind tunnel experiments [81] could be used.

Figure 9 depicts the C_T and C_Q variation of a single blade throughout a complete 360° azimuth at TSR = 3.3, as predicted by high-fidelity LBM and mid-fidelity LLFVW methods. The average values of C_T and C_Q are also shown. For both upwind and downwind parts of the rotation, both C_T and C_Q decrease monotonically with an increase in the number of blades due to increased blade-wake and blade-vortex interactions, leading to degraded individual blade aerodynamic efficiency. The downstream blades produce lower thrust and torque than the upstream blades, with the contribution from the latter, as part of the overall rotor, increasing as the number of blades increases. The results also reveal that the 4-bladed rotor produces negative torque for a significant portion of the downwind rotation, demonstrating the extent of blade-wake interaction in high-blade-number VAWTs. The mid-fidelity LLFVW and high-fidelity LBM both model these physical characteristics well. However, there is a mismatch in peak values between LLFVW and LBM for C_T and C_Q values, with LLFVW predicting lower values, and this mismatch improves slightly with an increase in the number of blades. Additionally, the study demonstrates that LBM exhibits a more pronounced reduction in blade performance with an increase in the number of blades, than LLFVW, highlighting a potential disadvantage of vortex-based methods in modelling unsteady aerodynamic interactions and wake dynamics.

The above-mentioned unsteady force field characteristics can also be visualised from Figure 10, showing the variation

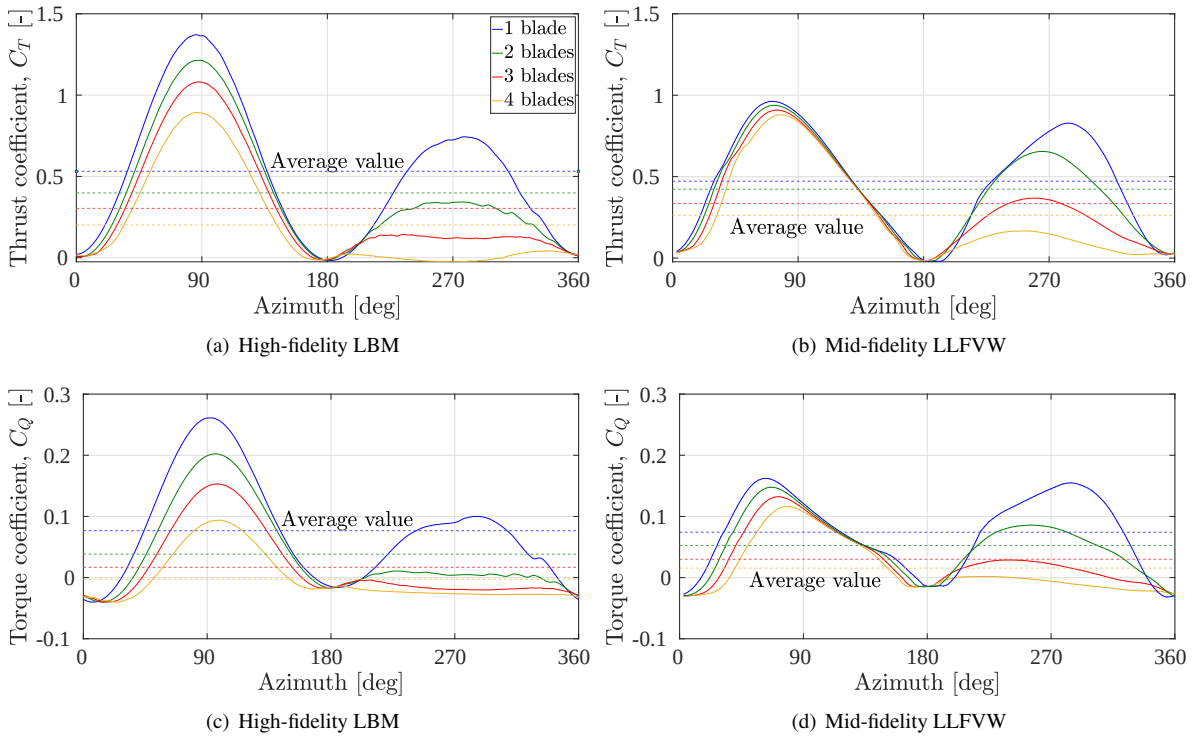

(a) High-fidelity LBM (b) Mid-fidelity LLFVW

(c) High-fidelity LBM (d) Mid-fidelity LLFVW

Fig. 9 Variation of thrust coefficient C_T and torque coefficient C_Q for a single blade over a complete rotation, using the high-fidelity LBM and mid-fidelity LLFVW at TSR = 3.3

in blade normal forces (F_n) over the equivalent 3D cylindrical surface traced by the VAWT blades at TSR = 3.3. Both azimuthal and spanwise directions are compared for all four VAWT configurations between LBM and LLFVW. The analysis indicates that normal blade forces degrade in the downwind part of rotation as compared to the upwind part, which is well captured by both methods for all VAWT configurations. Furthermore, the decrease in peak normal forces and the increase in the contribution of the upwind part, as compared to the downwind part, with an increase in the number of blades are also observed. However, there are two key differences between the two methods. Firstly, LLFVW predicts lower peak values of normal blade forces in both the upwind and downwind parts of rotation as compared to LBM, as also seen in the thrust and torque values of a single blade and overall rotor seen earlier in Figures 9 and 8, respectively. Secondly, the 3D effects of tip vortices on the force field are more pronounced with LBM than with LLFVW, as can be seen around h/H of -0.5 and 0.5 in Figure 10. These observations further support the conclusion that mid-fidelity vortex methods may not accurately model 3D fluid dynamic interactions, although their trends are consistent with those of the high-fidelity LBM method.

In order to gain a deeper understanding of the impact of blade-wake and blade-vortex interactions on overall rotor performance, it is essential to visualise the 3D VAWT flowfield. Figure 11 provides insight into instantaneous vortices in the downstream part of the VAWT flowfield using iso-surfaces of the λ_2 criterion for TSR = 3.3. The size of the large vortex structures, consisting of the coherent shed and trailing (tip) vortices, and smaller incoherent vortex structures, increases proportionately in the flowfield as the number of blades increases. Shed vortices originate at 0° and 180° azimuth due to the change in the direction of airflow around the blade as it moves from the downwind to the upwind part of rotation and vice versa. The coherent tip vortices shed from the tip of each blade are particularly significant, and their effects can be observed in Figure 10 around h/H of -0.5 and 0.5. These tip vortices convect downstream and create a spiral flow pattern, also known as a "vortex ring," that wraps around the turbine's axis. The density of these vortices in the vortex ring increases as the number of blades increases.

The convective motion of the large vortex structures downstream is accompanied by wake expansion and progressive disintegration into smaller-scale structures caused by flow instabilities and spatial modulation, which eventually dissipate and mix with the ambient fluid [82, 83]. As the number of blades increases, the increase in blade vortex interaction disturbs the ideal pressure and loading distribution along the chordwise and spanwise directions, leading to the lower

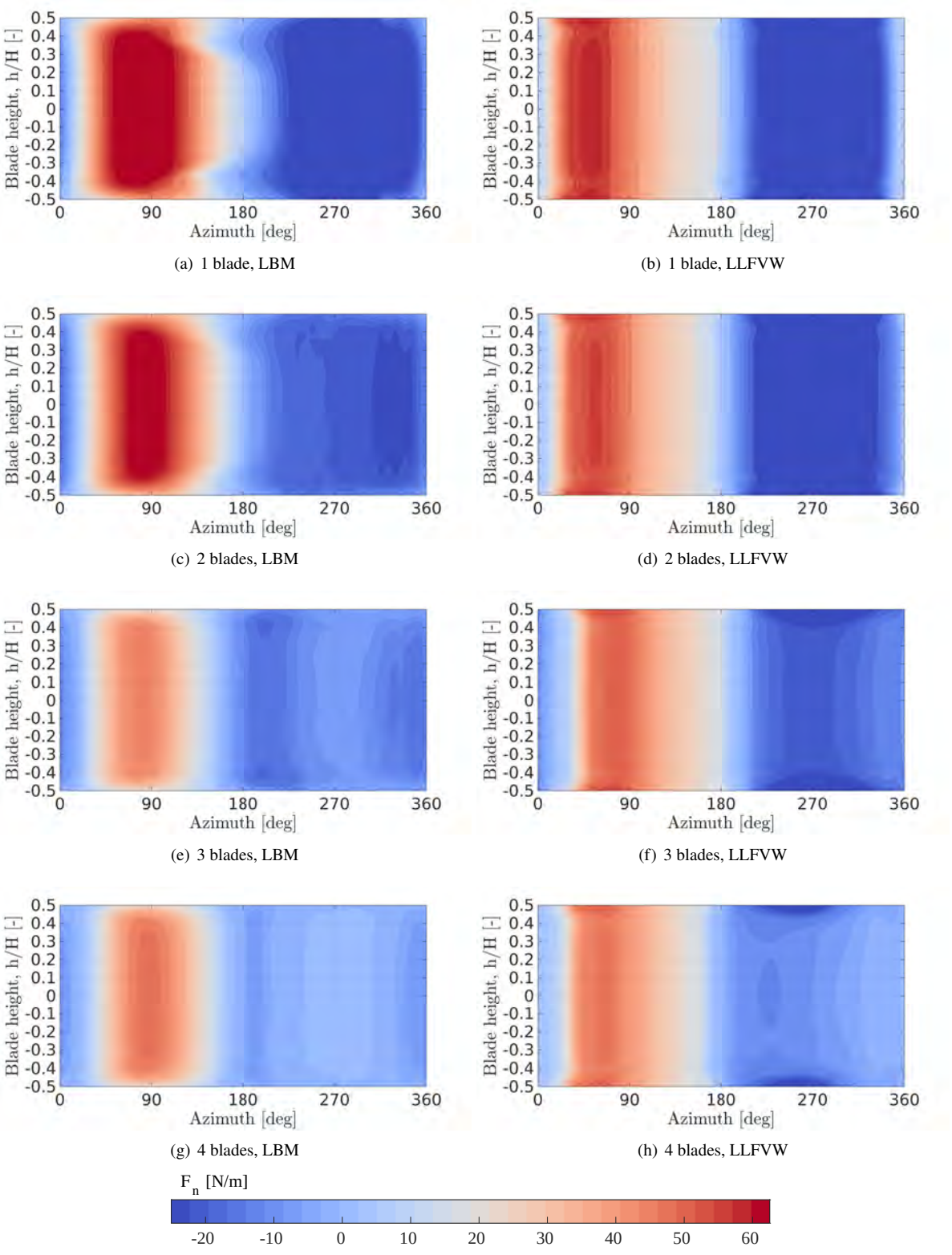

(a) 1 blade, LBM

(b) 1 blade, LLFVW

(c) 2 blades, LBM

(d) 2 blades, LLFVW

(e) 3 blades, LBM

(f) 3 blades, LLFVW

(g) 4 blades, LBM

(h) 4 blades, LLFVW

Fig. 10 Normal force contour for a single blade over azimuthal and spanwise directions, using the high-fidelity LBM and mid-fidelity LLFVW, at TSR = 3.3

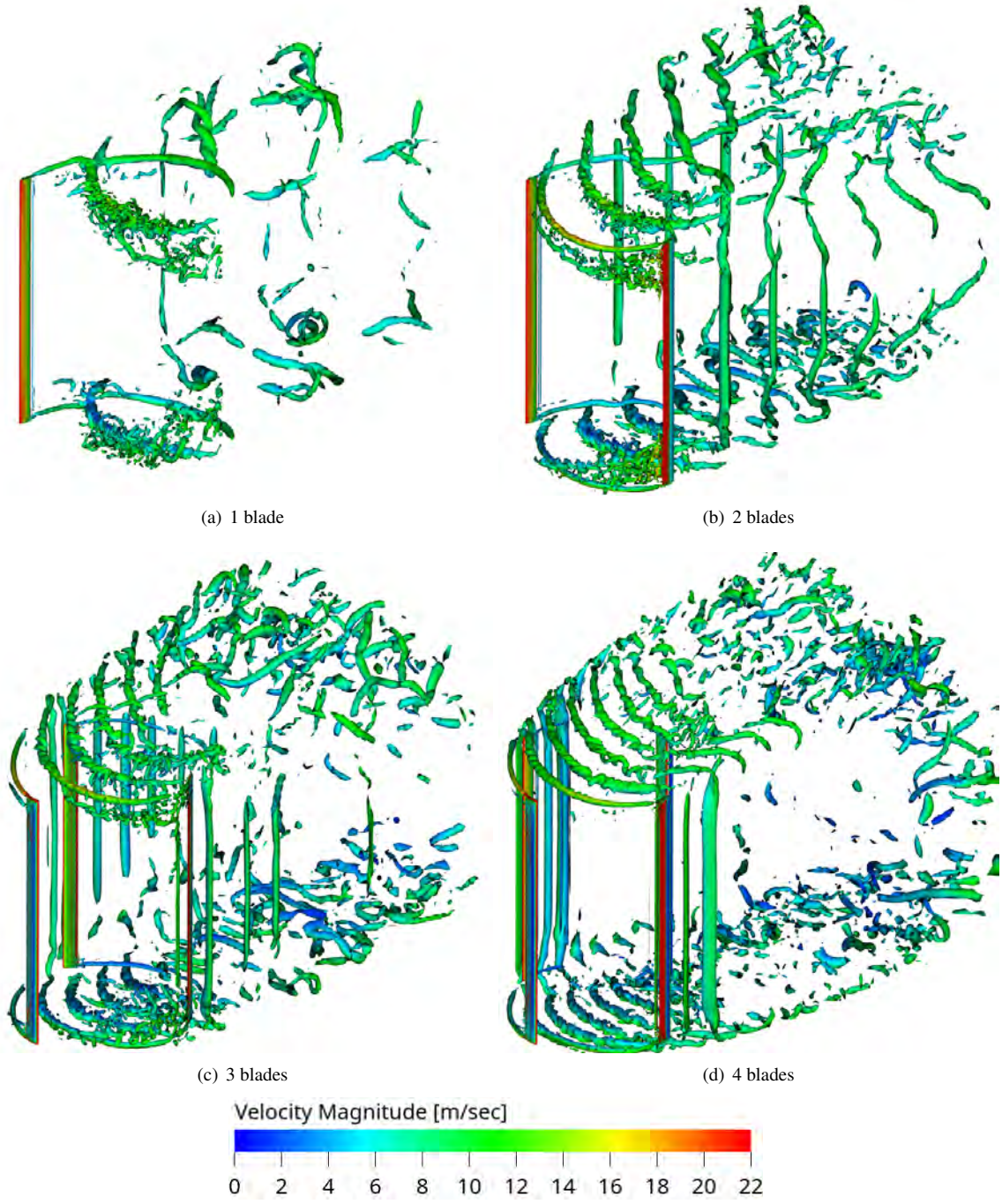

Fig. 11 Instantaneous 3D flowfield using iso-surfaces of the λ_2 criterion for vortices visualization, using high-fidelity LBM, at TSR = 3.3

aerodynamic performance of the downstream blades compared to the upstream blades (as observed earlier in Figures 8 and 9) which are exposed to undisturbed freestream flow.

Furthermore, as the number of blades increases, the downstream wake becomes stronger, resulting in lower streamwise velocity values. This phenomenon is illustrated in Figure 12, which displays the instantaneous streamwise velocity contours in the VAWT wake on a 2D plane located at the blade mid-span location, using both LBM and LLFVW methods for TSR = 3.3.

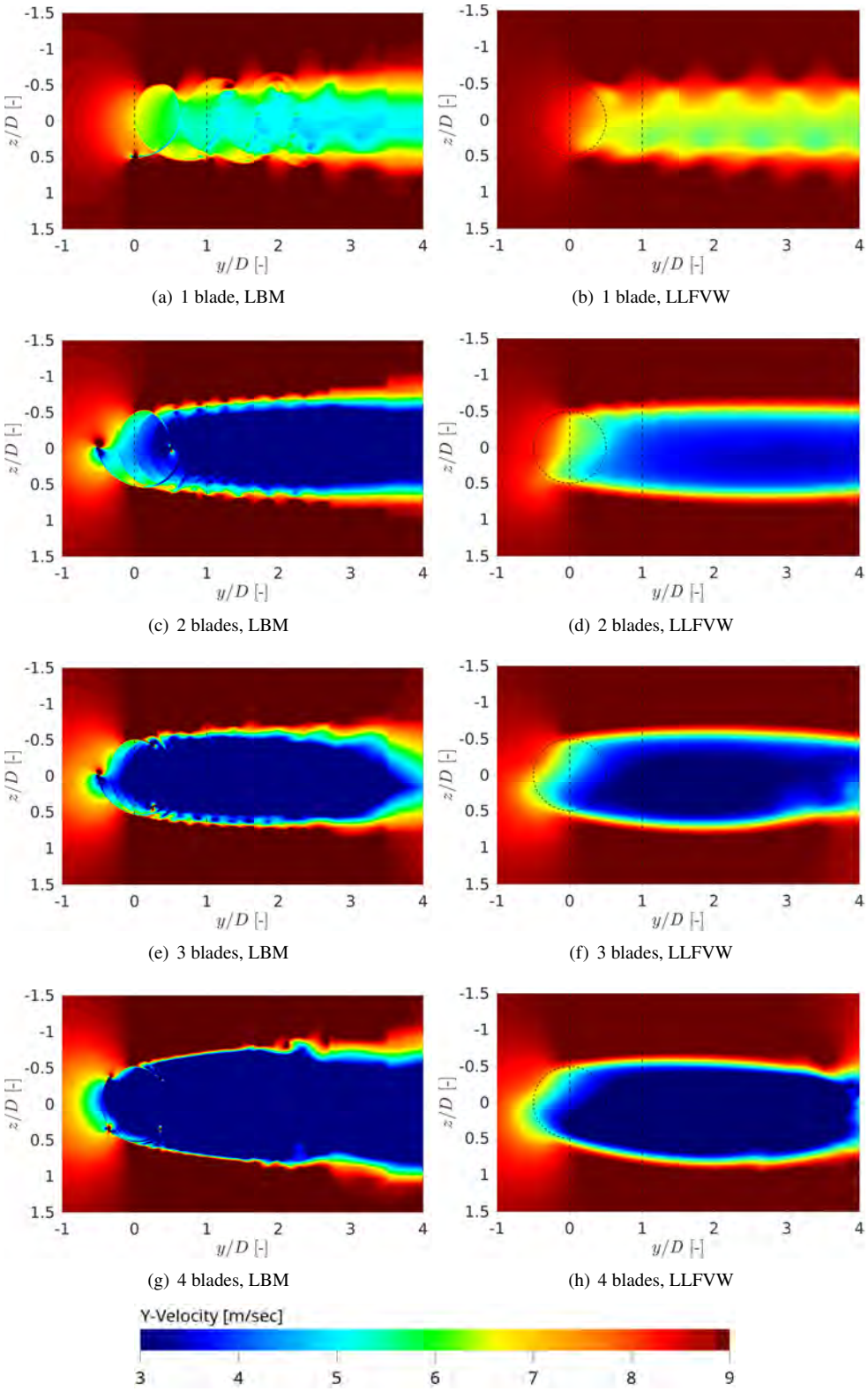

(a) 1 blade, LBM (b) 1 blade, LLFVW

(c) 2 blades, LBM (d) 2 blades, LLFVW

(e) 3 blades, LBM (f) 3 blades, LLFVW

(g) 4 blades, LBM (h) 4 blades, LLFVW

Fig. 12 Instantaneous streamwise velocity contours in the VAWT wake on a 2D plane located at the blade mid-span location, using both LBM and LLFVW methods at TSR = 3.3

The increase in blade number leads to more blockage to the flow, reducing the velocity induced at the upstream blades, and this effect is further magnified at the downstream blades. Consequently, the aerodynamic performance of downstream blades is inferior to that of the upstream blades, as evidenced by the results of thrust, torque and blade normal forces presented in Figures 8, 9 and 10. Both LBM and LLFVW methods capture the reduction in streamwise velocities with increasing blade numbers, but LLFVW predicts higher velocity values, and therefore less strong wake, compared to LBM. This trend is consistent for all simulated VAWT configurations.

The strength of the downstream wake proportionately increases with the strength of the force distribution on an airfoil or blade, such that an increase in blade number leads to a stronger wake, which is consistent with the increase in overall rotor thrust shown in Figure 8. Moreover, the 2D vortex structures illustrated in Figure 12 for LBM are more prominent than those for LLFVW. These structures are indicative of shed vortices, as demonstrated by a 3D view presented in Figure 11, and the differences in vortex modelling approaches suggest that LBM is more effective in capturing the blade vortex interaction.

After examining the wake characteristics of a VAWT in this study, it was found that the width of the velocity deficit region at any downstream location in the near-wake increases with the number of blades. This result is consistent across all simulations conducted using both the LBM and LLFVW methods. This is demonstrated in Figure 13, which shows the streamwise velocity values averaged over a rotation. The values are plotted along lines situated at distances of $0D$ and $1D$ downstream from the VAWT centre at the blade-mid-span 2D plane and are illustrated in Figure 12 as black dotted lines. Tavernier [84] similarly concluded using the Actuator Cylinder Theory when the ratio of loading in the upwind to downwind half of rotation increases, resulting in a wider velocity deficit region, which is what happens when the number of blades increases.

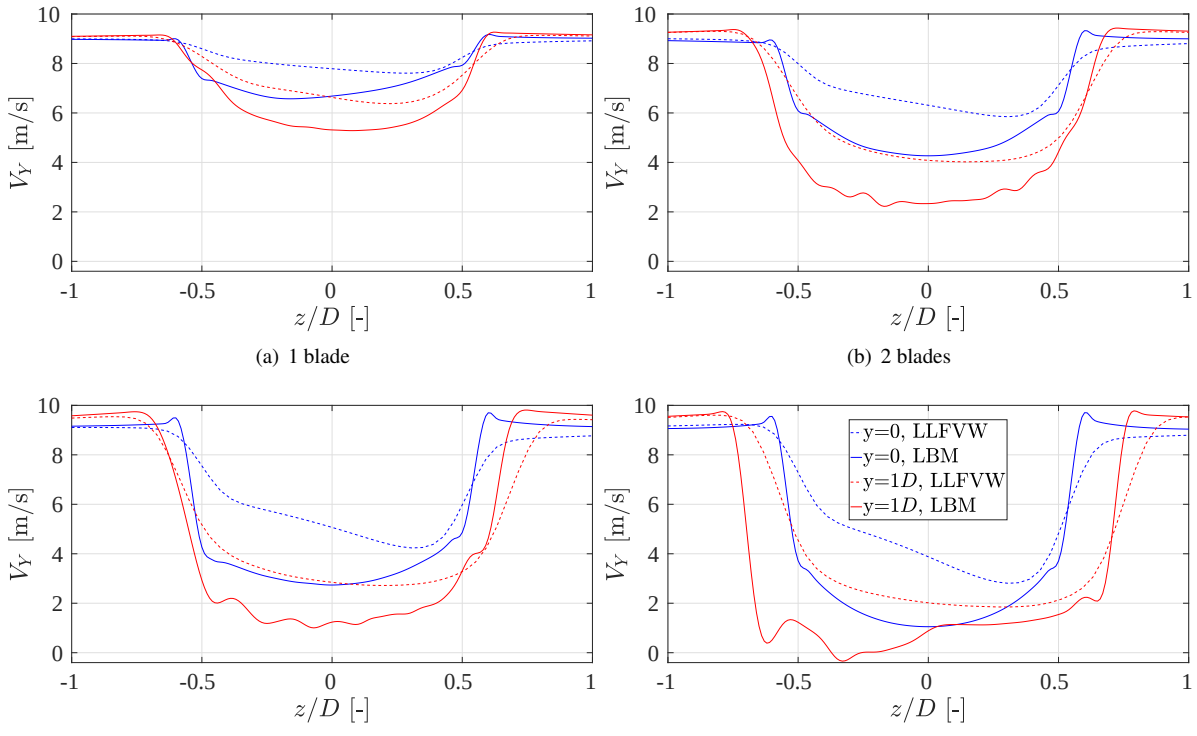

(a) 1 blade (b) 2 blades

(c) 3 blades (d) 4 blades

Fig. 13 Comparison of streamwise velocities, averaged over a rotation, in the downstream VAWT flowfield using high-fidelity LBM and mid-fidelity LLFVW at two different locations at TSR = 3.3

The LLFVW method is found to predict higher streamwise velocities compared to LBM, especially at the centre of the wake. In addition, the asymmetrical nature of the VAWT flow field is observed across all configurations, as demonstrated by both methods used. Figure 14 visualises the instantaneous streamwise velocities experienced by the VAWT blade at the most upstream (90°) and most downstream location (270°) for the 1-bladed and 3-bladed VAWT configurations using high-fidelity LBM. An increase in the number of blades leads to a reduction in the induced velocity

experienced by the upstream blade, which in turn results in a decrease in blade angle of attack (AoA) and aerodynamic performance. The induced velocity further decreases for the downstream blades, resulting in an even lower AoA. These variations in streamwise velocities are consistent with the results presented in Figure 12 on a larger scale of the overall rotor wake.

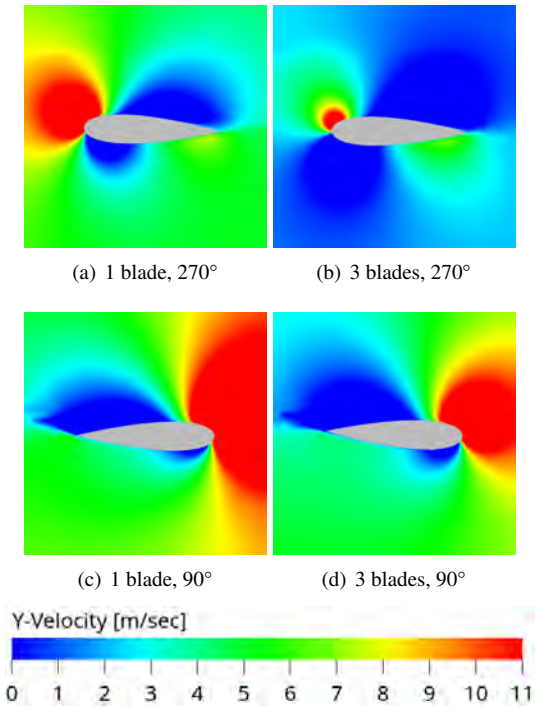

Fig. 14 Comparison of instantaneous velocities experienced by the blade at the most upstream (90°) and the most downstream location (270°) for the 1- and 3-bladed configurations, using the high-fidelity LBM at TSR = 3.3

Figure 15 reports unsteady pressure data from the VAWT obtained at two different locations, one at the rotor plane ([0,0,7D]) and one out of the rotor plane ([4D,0,7D]), over a single rotor rotation obtained using high-fidelity LBM. Both Figures 15 (a) and (b) show that an increase in the number of blades results in a decrease in the amplitude of pressure fluctuations at both locations. This decrease is attributed to the reduction in the unsteady fluctuations in overall rotor loading or thrust values, as previously shown in Figure 8. Additionally, the in-plane location exhibits more prominent high-frequency pressure fluctuations than the out-of-plane location.

In Figure 15 (c), it is observed that the pressure fluctuations from a single blade increase proportionately with the individual blade loading, with the highest fluctuations obtained for the case of a 1-bladed rotor. Additionally, Figure 15 (d) shows the individual contribution from both blades of a 2-bladed rotor, shifted by a phase angle of 180°. The level of constructive and/or destructive interference in the pressure fluctuations can be seen from this figure. For 3-bladed and 4-bladed rotors, a similar phase shift of 120° and 90°, respectively, will be obtained.

Figure 16 reports the sound pressure level (SPL) values in dB/Hz over a frequency range of 20-2000 Hz obtained using high-fidelity LBM, at the two observer locations considered in this study. The results indicate that the SPL values for the 1-bladed and 2-bladed VAWTs are higher in the low-frequency range (20-40 Hz) compared to the other configurations. This is attributed to the contribution of tonal blade passage frequency (BPF) noise, which arises due to the larger amplitude of azimuthal rotor loading for these VAWTs as indicated in Figure 8. Conversely, the 3-bladed and 4-bladed VAWTs produce more noise in the mid and high-frequency ranges. This observation is supported by the pressure fluctuations data presented in Figure 15 (a) and (b), where high-frequency pressure fluctuations are significantly higher in the 3-bladed and 4-bladed configurations than the other configurations. It is important to note that the noise levels are generally higher at the in-plane location than at the out-of-plane location.

Figure 17 presents the directivity plot of the overall sound pressure level (OSPL) comparing VAWTs with varying number of blades at TSR of 3.3. The OSPL values are obtained using high-fidelity LBM and are calculated within the frequency range of 20-2000 Hz. For both the YZ and XY planes, noise levels exhibit an increasing trend with an

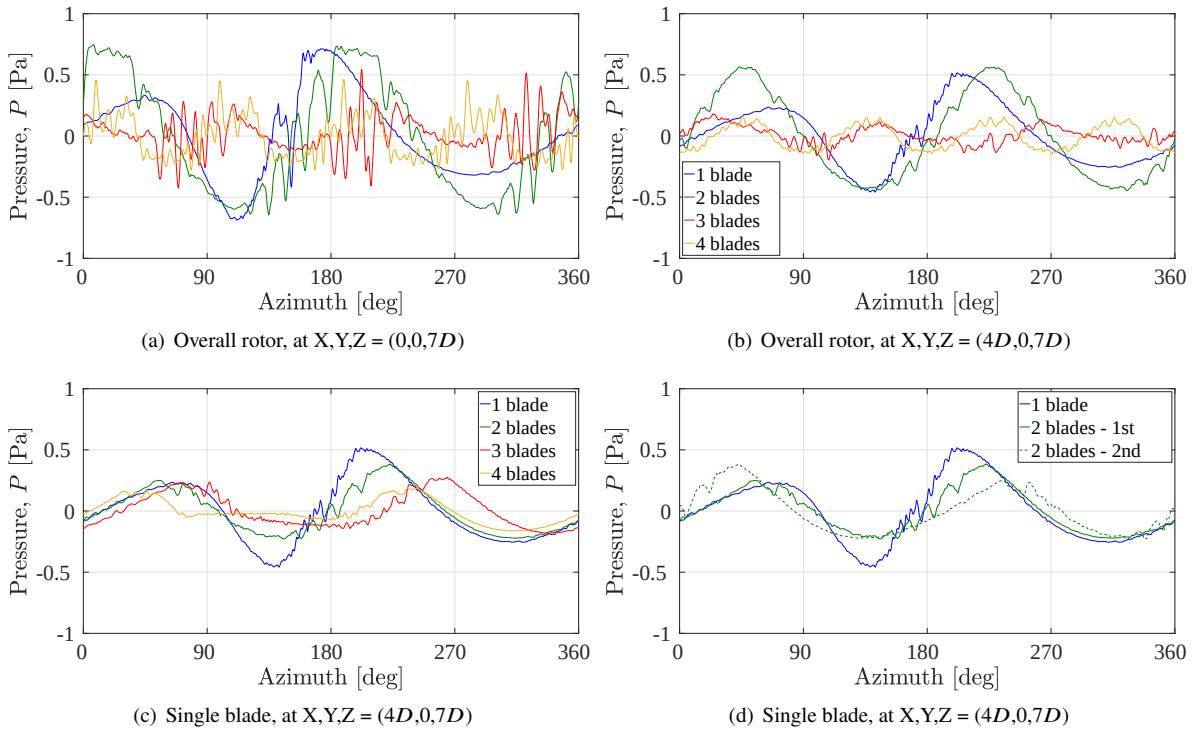

(a) Overall rotor, at X,Y,Z = (0,0,7D)

(b) Overall rotor, at X,Y,Z = (4D,0,7D)

(c) Single blade, at X,Y,Z = (4D,0,7D)

(d) Single blade, at X,Y,Z = (4D,0,7D)

Fig. 15 Raw unsteady pressure data for different VAWT configurations using the high-fidelity LBM at TSR = 3.3

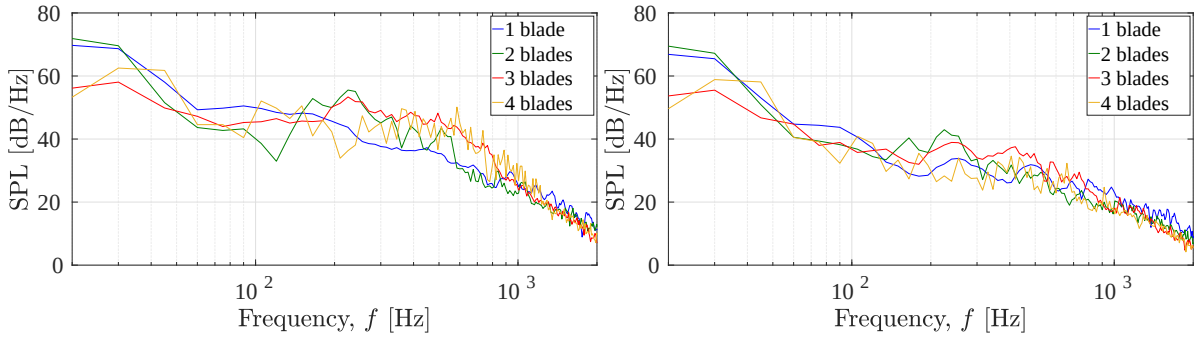

(a) At X,Y,Z = (0,0,7D)

(b) At X,Y,Z = (4D,0,7D)

Fig. 16 Sound Pressure Level (SPL) spectra using the high-fidelity LBM at two different locations at TSR = 3.3

increase in the number of blades until the 3-bladed rotor, after which it decreases for the 4-bladed rotor. This observation can be linked to the overall rotor thrust values depicted in Figure 7, where the VAWT thrust decreases for the 4-bladed rotor following a monotonic increase up to the 3-bladed rotor. It should be noted that this study focuses on VAWTs operating in a low Reynolds number regime, where blade loading noise is the predominant noise source [85].

On the YZ plane, both the 3-bladed and 4-bladed VAWTs exhibit an increase in noise levels at 180° azimuth, while a decrease is observed at 0° azimuth. In contrast, the 1-bladed and 2-bladed VAWTs demonstrate relatively constant noise levels throughout the entire 360° azimuth range. There are various noise sources in a VAWT [41, 79, 86, 87] and the observed discrepancy indicates that some noise sources are more dominant in the former configurations as compared to the latter configurations. Further investigation utilizing low-fidelity aeroacoustic prediction models [52] can provide valuable insights into the specific contributions of different noise sources for different number of blades.

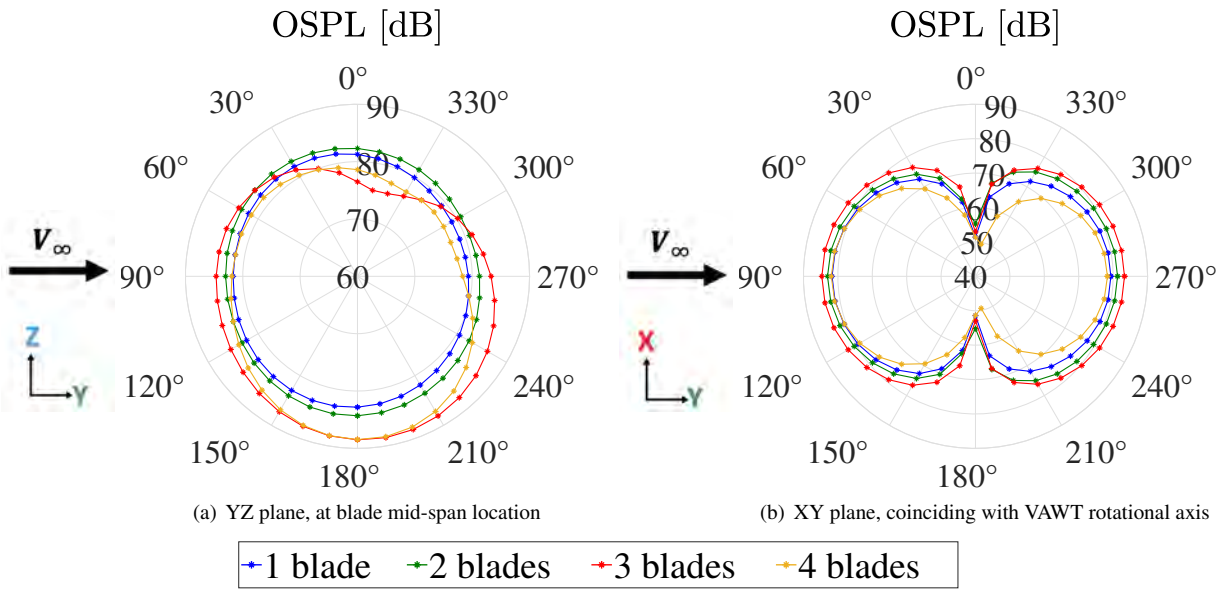

(a) YZ plane, at blade mid-span location

(b) XY plane, coinciding with VAWT rotational axis

Fig. 17 Directivity plot of overall sound pressure level (OSPL) comparing VAWTs with different number of blades at TSR = 3.3, along a circular array of 36 points situated at a distance of 7D from the origin of VAWT ([0,0,0])

V. Conclusions

This study presents a comprehensive investigation of the impact of the number of blades on the aerodynamic and aeroacoustic properties of Darrieus vertical axis wind turbines (VAWTs). The research aims to achieve two objectives: to facilitate the creation of a multi-fidelity simulation framework for VAWT optimization, and to examine the influence of number of blades on VAWT performance. High-fidelity Lattice Boltzmann Method (LBM) 3D aerodynamic simulations are conducted, and far-field noise is calculated using the Ffowcs Williams and Hawkings (FW-H) methodology. Additionally, mid-fidelity simulations using the Lifting Line Free Vortex Wake (LLFVW) method are performed. The investigation concentrates on examining the impact of number of blades on thrust and power performance, as well as far-field noise. Furthermore, the study compares the 3D force-field and flow-field outcomes obtained with mid-fidelity and high-fidelity approaches and identifies potential differences in the modeling of fluid dynamic interactions that may result in variations in the results.

A straight-bladed Darrieus VAWT, with geometrical parameters replicated from the study conducted by Balduzzi et al. [45], is employed in this study. The rotor configurations considered include 1-bladed, 2-bladed, 3-bladed, and 4-bladed rotors, with a solidity of 0.08 for the 1-bladed rotor and increasing proportionally to the number of blades. The rotor aspect ratio for all configurations is 1.46. The LLFVW method is used to simulate a range of Tip Speed Ratios (TSRs), while the LBM is used to simulate a TSR of 3.3 for all four geometries. Statistical temporal convergence is achieved earlier for the 1-bladed rotor than for the 3-bladed rotor, for both methods, and confirmed by low uncertainty (u) values. Grid convergence results reveal that the thrust values exhibit better grid convergence than the torque values. The finest of the four grids simulated exhibits the most favourable grid convergence and is subsequently chosen for further flow physics analysis. For validation purposes, the power coefficient (C_P) values obtained using LBM and LLFVW methods are compared with reference data reported by Balduzzi et al. [45], and the results show excellent agreement.

The investigation found that the number of blades in a VAWT influences power generation, with more blades (higher solidity) producing more power at lower TSRs, while fewer blades produce more power at higher TSRs. At low TSRs, increasing the solidity has little effect on blade-wake/blade-vortex interaction, resulting in increased blade tangential loading and power production. Conversely, at higher TSRs, increasing the solidity worsens the tangential loading and reduces rotor power. Consequently, higher solidity results in a steeper C_P gradient than lower solidity cases across the entire range of TSR. The optimal TSR decreases as the number of blades increases, as indicated by C_P values. Initially, C_T increases with increasing TSR and blade number, but it slightly decreases at high TSR and for the 4-bladed rotor. The study also shows that as the number of blades increases, the amplitude of variation in thrust and torque values decreases, resulting in smoother overall rotor loading variations.

The physical trends mentioned above are well captured by both the mid-fidelity LLFVW and high-fidelity LBM methods. However, LLFVW predicts lower peak C_T and C_Q values in the upwind and downwind regions compared to LBM, except for the 2-bladed rotor where there is a good agreement. This discrepancy also exists when comparing blade normal forces and streamwise velocities in the downstream near-wake region. This suggests that LLFVW may not capture the complex 3D effects in VAWT flow and force fields as strongly as LBM, particularly as the number of blades increases. As a result, the former predicts higher thrust and power values of the overall rotor compared to the latter. The study suggests empirical modifications in the airfoil lift and drag polar values for the LLFVW method. The aeroacoustic characteristics of all four VAWT configurations are also compared in the study. The low-frequency BPF noise was found to be higher in VAWTs with fewer blades, due to the higher rotor loading or thrust values obtained. Whereas, the high-frequency noise was found to be higher in VAWTs with more blades, due to a higher intensity of BVI between the downstream blades and previously shed blade vortices. OSPL directivity plot revealed that overall noise increased with an increase in the number of blades except for the 4-bladed VAWT for which the noise decreased.

This study examined the impact of one of the design parameters, the number of blades, on VAWT performance and noise generation. However, given the large 3D design space of VAWTs, further investigation is necessary to assess the impact of other geometric parameters, such as the central tower and supporting struts, aspect ratio, blade design, as well as flow parameters, including non-uniform inflow, on aerodynamic performance and noise generation. Low-fidelity aeroacoustic prediction studies are also suggested to understand the significance of different noise sources for different VAWT configurations and operating conditions. Furthermore, it is essential to compare multi-fidelity approaches for aerodynamics and aeroacoustics in all of the aforementioned studies. Accurate predictions by low-to-mid fidelity models are crucial for efficient VAWT design optimization, improving power characteristics and reducing noise.

Acknowledgments

This project has received funding from the European Union's Horizon 2020 Marie Curie zEPHYR research and innovation programme under grant agreement No EC grant 860101 (https://www.h2020-zephyr.eu/). Nottingham Trent University has received sponsorship from 3DS Simulia for the commercial software PowerFLOW. Special thanks to a few researchers for a thoughtful discussion on the PowerFLOW simulations - Gianluca Romani and Edoardo Grande, and on the QBlade simulations - Adhyanth Giri Ajay and David Marten; and thanks to Damiano Casalino for sharing with me his *optydb* tool.

References

[1] Desa, U. N., "World urbanization prospects: the 2018 revision, key facts," *New York: NY. Available online at: https://population. un. org/wup/Publications/(Accessed December 20, 2018)*, 2018.

[2] Van Kuik, G., Peinke, J., Nijssen, R., Lekou, D., Mann, J., Sørensen, J. N., Ferreira, C., van Wingerden, J.-W., Schlipf, D., Gebraad, P., et al., "Long-term research challenges in wind energy–a research agenda by the European Academy of Wind Energy," *Wind energy science*, Vol. 1, No. 1, 2016, pp. 1–39.

[3] Quintero Pulido, D. F., Ten Kortenaar, M. V., Hurink, J. L., and Smit, G. J., "The role of off-grid houses in the energy transition with a case study in the Netherlands," *Energies*, Vol. 12, No. 10, 2019, p. 2033.

[4] Micallef, D., and Van Bussel, G., "A review of urban wind energy research: aerodynamics and other challenges," *Energies*, Vol. 11, No. 9, 2018, p. 2204.

[5] Kumar, R., Raahemifar, K., and Fung, A. S., "A critical review of vertical axis wind turbines for urban applications," *Renewable and Sustainable Energy Reviews*, Vol. 89, 2018, pp. 281–291.

[6] Dabiri, J. O., "Potential order-of-magnitude enhancement of wind farm power density via counter-rotating vertical-axis wind turbine arrays," *Journal of renewable and sustainable energy*, Vol. 3, No. 4, 2011, p. 043104.

[7] Wilson, R. E., and Lissaman, P. B., "Applied aerodynamics of wind power machines," *National Science Foundation*, 1974.

[8] Le Gourieres, D., *Wind power plants: theory and design*, Elsevier, 2014.

[9] Bakker, R. H., Pedersen, E., van den Berg, G. P., Stewart, R. E., Lok, W., and Bouma, J., "Impact of wind turbine sound on annoyance, self-reported sleep disturbance and psychological distress," *Science of the total environment*, Vol. 425, 2012, pp. 42–51.

[10] Klæboe, R., and Sundfør, H. B., "Windmill noise annoyance, visual aesthetics, and attitudes towards renewable energy sources," *International journal of environmental research and public health*, Vol. 13, No. 8, 2016, p. 746.

[11] Roh, S.-C., and Kang, S.-H., "Effects of a blade profile, the Reynolds number, and the solidity on the performance of a straight bladed vertical axis wind turbine," *Journal of Mechanical Science and Technology*, Vol. 27, No. 11, 2013, pp. 3299–3307.

[12] Maeda, T., Kamada, Y., Murata, J., Furukawa, K., Yamamoto, M., et al., "Effect of number of blades on aerodynamic forces on a straight-bladed Vertical Axis Wind Turbine," *Energy*, Vol. 90, 2015, pp. 784–795.

[13] Li, Q., Maeda, T., Kamada, Y., Murata, J., Kawabata, T., Furukawa, K., and Kogaki, T., "Effect of blade number on flow around straight-bladed vertical axis wind turbine," *Transactions of the JSME (in Japanese)*, Vol. 80, No. 816, 2014.

[14] Maeda, T., Kamada, Y., Murata, J., Shimizu, K., Ogasawara, T., Nakai, A., Kasuya, T., et al., "Effect of solidity on aerodynamic forces around straight-bladed vertical axis wind turbine by wind tunnel experiments (depending on number of blades)," *Renewable energy*, Vol. 96, 2016, pp. 928–939.

[15] Qu, J., Xu, M., and Li, Y., "Effects of blade number on self-starting performance of vertical axis wind turbine with self-adapting wind speed under low wind speed," *Transactions of the Chinese Society for Agricultural Machinery*, Vol. 5, 2014, pp. 173–178.

[16] Sunyoto, A., Wenehenubun, F., and Sutanto, H., "The effect of number of blades on the performance of H-Darrieus type wind turbine," *2013 International Conference on QiR*, IEEE, 2013, pp. 192–196.

[17] Howell, R., Qin, N., Edwards, J., and Durrani, N., "Wind tunnel and numerical study of a small vertical axis wind turbine," *Renewable energy*, Vol. 35, No. 2, 2010, pp. 412–422.

[18] Delafin, P.-L., Nishino, T., Wang, L., and Kolios, A., "Effect of the number of blades and solidity on the performance of a vertical axis wind turbine," *Journal of Physics: Conference Series*, Vol. 753, IOP Publishing, 2016, p. 022033.

[19] Mohamed, M., "Performance investigation of H-rotor Darrieus turbine with new airfoil shapes," *Energy*, Vol. 47, No. 1, 2012, pp. 522–530.

[20] Sun, X., Zhu, J., Li, Z., and Sun, G., "Rotation improvement of vertical axis wind turbine by offsetting pitching angles and changing blade numbers," *Energy*, Vol. 215, 2021, p. 119177.

[21] Rezaeiha, A., Montazeri, H., and Blocken, B., "Towards optimal aerodynamic design of vertical axis wind turbines: Impact of solidity and number of blades," *Energy*, Vol. 165, 2018, pp. 1129–1148.

[22] Castelli, M. R., De Betta, S., and Benini, E., "Effect of blade number on a straight-bladed vertical-axis Darreius wind turbine," *International Journal of Aerospace and Mechanical Engineering*, Vol. 6, No. 1, 2012, pp. 68–74.

[23] Tangler, J., "The evolution of rotor and blade design," Tech. rep., National Renewable Energy Lab.(NREL), Golden, CO (United States), 2000.

[24] Lam, H., Liu, Y., Peng, H., Lee, C., and Liu, H., "Assessment of solidity effect on the power performance of H-rotor vertical axis wind turbines in turbulent flows," *Journal of Renewable and Sustainable Energy*, Vol. 10, No. 2, 2018, p. 023304.

[25] Eboibi, O., Danao, L. A. M., and Howell, R. J., "Experimental investigation of the influence of solidity on the performance and flow field aerodynamics of vertical axis wind turbines at low Reynolds numbers," *Renewable Energy*, Vol. 92, 2016, pp. 474–483.

[26] Maeda, T., Kamada, Y., Shimizu, K., Ogasawara, T., Nakai, A., Kasuya, T., et al., "Effect of rotor aspect ratio and solidity on a straight-bladed vertical axis wind turbine in three-dimensional analysis by the panel method," *Energy*, Vol. 121, 2017, pp. 1–9.

[27] Xisto, C. M., Páscoa, J. C., and Trancossi, M., "Geometrical parameters influencing the aerodynamic efficiency of a small-scale self-pitch high-solidity VAWT," *Journal of Solar Energy Engineering*, Vol. 138, No. 3, 2016, p. 031006.

[28] Hassan, S. R., Ali, M., and Islam, M. Q., "The effect of solidity on the performance of H-Rotor Darrieus turbine," *AIP Conference Proceedings*, Vol. 1754, AIP Publishing LLC, 2016, p. 040012.

[29] Mohamed, M., "Impacts of solidity and hybrid system in small wind turbines performance," *Energy*, Vol. 57, 2013, pp. 495–504.

[30] Subramanian, A., Yogesh, S. A., Sivanandan, H., Giri, A., Vasudevan, M., Mugundhan, V., and Velamati, R. K., "Effect of airfoil and solidity on performance of small scale vertical axis wind turbine using three dimensional CFD model," *Energy*, Vol. 133, 2017, pp. 179–190.

[31] Sagharichi, A., Zamani, M., and Ghasemi, A., "Effect of solidity on the performance of variable-pitch vertical axis wind turbine," *Energy*, Vol. 161, 2018, pp. 753–775.

[32] Li, S., and Li, Y., "Numerical study on the performance effect of solidity on the straight-bladed vertical axis wind turbine," *2010 Asia-Pacific power and energy engineering conference*, IEEE, 2010, pp. 1–4.

[33] Möllerström, E., Ottermo, F., Hylander, J., and Bernhoff, H., "Noise emission of a 200 kW vertical axis wind turbine," *Energies*, Vol. 9, No. 1, 2016, p. 19.

[34] Möllerström, E., Larsson, S., Ottermo, F., Hylander, J., and Bååth, L., "Noise propagation from a vertical axis wind turbine," *inter. noise 2014, 43rd International Congress on Noise Control Engineering, Melbourne, Australia, November 16-19, 2014*, Australian Acoustical Society, 2014.

[35] Dumitrescu, H., Cardos, V., Dumitrache, A., and Frunzulica, F., "Low-frequency noise prediction of vertical axis wind turbines," *Proceedings of the Romanian Academy*, Vol. 11, No. 1, 2010, pp. 47–54.

[36] Mohamed, M., "Aero-acoustics noise evaluation of H-rotor Darrieus wind turbines," *Energy*, Vol. 65, 2014, pp. 596–604.

[37] Mohamed, M., "Criticism study of J-Shaped Darrieus wind turbine: Performance evaluation and noise generation assessment," *Energy*, Vol. 177, 2019, pp. 367–385.

[38] Rasekh, S., and Karimian, S., "Effect of solidity on aeroacoustic performance of a vertical axis wind turbine using improved delayed detached eddy simulation," *International Journal of Aeroacoustics*, Vol. 20, No. 3-4, 2021, pp. 390–413.

[39] Mohamed, M., "Reduction of the generated aero-acoustics noise of a vertical axis wind turbine using CFD (Computational Fluid Dynamics) techniques," *Energy*, Vol. 96, 2016, pp. 531–544.

[40] Ghasemian, M., and Nejat, A., "Aero-acoustics prediction of a vertical axis wind turbine using Large Eddy Simulation and acoustic analogy," *Energy*, Vol. 88, 2015, pp. 711–717.

[41] Botha, J., Shahroki, A., and Rice, H., "An implementation of an aeroacoustic prediction model for broadband noise from a vertical axis wind turbine using a CFD informed methodology," *Journal of Sound and Vibration*, Vol. 410, 2017, pp. 389–415.

[42] Su, J., Lei, H., Zhou, D., Han, Z., Bao, Y., Zhu, H., and Zhou, L., "Aerodynamic noise assessment for a vertical axis wind turbine using Improved Delayed Detached Eddy Simulation," *Renewable energy*, Vol. 141, 2019, pp. 559–569.

[43] Dessoky, A., Bangga, G., Lutz, T., and Krämer, E., "Aerodynamic and aeroacoustic performance assessment of H-rotor darrieus VAWT equipped with wind-lens technology," *Energy*, Vol. 175, 2019, pp. 76–97.

[44] Marten, D., Bianchini, A., Pechlivanoglou, G., Balduzzi, F., Nayeri, C. N., Ferrara, G., Paschereit, C. O., and Ferrari, L., "Effects of airfoil's polar data in the stall region on the estimation of Darrieus wind turbine performance," *Journal of Engineering for Gas Turbines and Power*, Vol. 139, No. 2, 2017.

[45] Balduzzi, F., Marten, D., Bianchini, A., Drofelnik, J., Ferrari, L., Campobasso, M. S., Pechlivanoglou, G., Nayeri, C. N., Ferrara, G., and Paschereit, C. O., "Three-dimensional aerodynamic analysis of a Darrieus wind turbine blade using computational fluid dynamics and lifting line theory," *Journal of Engineering for Gas Turbines and Power*, Vol. 140, No. 2, 2018.

[46] Van Garrel, A., "Development of a wind turbine aerodynamics simulation module," 2003.

[47] Marten, D., "QBlade Guidelines v0. 95," *Technical University of Berlin, Berlin, Germany*, 2016.

[48] Marten, D., Lennie, M., Pechlivanoglou, G., Nayeri, C. N., and Paschereit, C. O., "Implementation, optimization, and validation of a nonlinear lifting line-free vortex wake module within the wind turbine simulation code qblade," *Journal of Engineering for Gas Turbines and Power*, Vol. 138, No. 7, 2016.

[49] Marten, D., Pechlivanoglou, G., Navid Nayeri, C., and Oliver Paschereit, C., "Nonlinear lifting line theory applied to vertical axis wind turbines: Development of a practical design tool," *Journal of Fluids Engineering*, Vol. 140, No. 2, 2018.

[50] Bergami, L., and Gaunaa, M., "ATEFlap Aerodynamic Model, a dynamic stall model including the effects of trailing edge flap deflection," 2012.

[51] Wendler, J., Marten, D., Pechlivanoglou, G., Nayeri, C. N., and Paschereit, C. O., "An unsteady aerodynamics model for lifting line free vortex wake simulations of hawt and vawt in qblade," *Turbo Expo: Power for Land, Sea, and Air*, Vol. 49873, American Society of Mechanical Engineers, 2016, p. V009T46A011.

[52] Brandetti, L., Avallone, F., De Tavernier, D., LeBlanc, B., Ferreira, C. S., and Casalino, D., "Assessment through high-fidelity simulations of a low-fidelity noise prediction tool for a vertical-axis wind turbine," *Journal of Sound and Vibration*, Vol. 547, 2023, p. 117486.

[53] Gourdain, N., Jardin, T., Serre, R., Prothin, S., and Moschetta, J.-M., "Application of a lattice Boltzmann method to some challenges related to micro-air vehicles," *International Journal of Micro Air Vehicles*, Vol. 10, No. 3, 2018, pp. 285–299.

[54] Avallone, F., van den Ende, L., Li, Q., Ragni, D., Casalino, D., Eitelberg, G., and Veldhuis, L., "Aerodynamic and aeroacoustic effects of swirl recovery vanes length," *Journal of Aircraft*, Vol. 56, No. 6, 2019, pp. 2223–2235.

[55] Casalino, D., Hazir, A., and Mann, A., "Turbofan broadband noise prediction using the lattice Boltzmann method," *AIAA Journal*, Vol. 56, No. 2, 2018, pp. 609–628.

[56] Nardari, C., Casalino, D., Polidoro, F., Coralic, V., Lew, P.-T., and Brodie, J., "Numerical and experimental investigation of flow confinement effects on UAV rotor noise," *25th AIAA/CEAS Aeroacoustics Conference*, 2019, p. 2497.

[57] Succi, S., *The lattice Boltzmann equation for fluid dynamics and beyond*, 1st ed., Clarendon Press, Oxford, 2001.

[58] Shan, X., Yuan, X.-F., and Chen, H., "Kinetic theory representation of hydrodynamics: a way beyond the Navier–Stokes equation," *Journal of Fluid Mechanics*, Vol. 550, 2006, pp. 413–441. https://doi.org/10.1017/S0022112005008153, URL http://www.journals.cambridge.org/abstract_S0022112005008153.

[59] Chen, S., and Doolen, G., "Lattice Boltzmann method for fluid flows," *Annual Review of Fluid Mechanics*, Vol. 30, No. 1, 1998, pp. 329–364. https://doi.org/10.1146/annurev.fluid.30.1.329, URL http://www.annualreviews.org/doi/10.1146/annurev.fluid.30.1.329.

[60] Chen, H., Chen, S., and Matthaeus, W., "Recovery of the Navier-Stokes equations using a lattice-gas Boltzmann method," *Physical Review A*, Vol. 45, No. 8, 1992, pp. R5339–R5342. https://doi.org/10.1103/PhysRevA.45.R5339, URL https://link.aps.org/doi/10.1103/PhysRevA.45.R5339.

[61] Chen, H., Zhang, R., and Gopalakrishnan, P., "Lattice Boltzmann Collision Operators Enforcing Isotropy and Galilean Invariance," , 8 2015. URL https://patents.google.com/patent/US20150356217A1/en.

[62] Yakhot, V., and Orszag, S., "Renormalization group analysis of turbulence. I. Basic theory," *Journal of Scientific Computing*, Vol. 1, No. 1, 1986, pp. 3–51. https://doi.org/10.1007/BF01061452, URL http://link.springer.com/10.1007/BF01061452.

[63] Teixeira, C., "Incorporating Turbulence Models into the Lattice-Boltzmann Method," *International Journal of Modern Physics C*, Vol. 09, No. 08, 1998, pp. 1159–1175. https://doi.org/10.1142/S0129183198001060, URL http://www.worldscientific.com/doi/abs/10.1142/S0129183198001060.

[64] Wilcox, D., *Turbulence modelling for CFD (Third Edition)*, DCW Industries, Incorporated, 2006.

[65] Launder, B., and Spalding, D., "The numerical computation of turbulent flows," *Computer Methods in Applied Mechanics and Engineering*, Vol. 3, No. 2, 1974, pp. 269–289. https://doi.org/10.1016/0045-7825(74)90029-2, URL http://www.sciencedirect.com/science/article/pii/0045782574900292.

[66] Ffowcs Williams, J. E., and Hawkings, D. L., "Sound generation by turbulence and surfaces in arbitrary motion," *Philosophical Transactions of the Royal Society of London. Series A, Mathematical and Physical Sciences*, Vol. 264, No. 1151, 1969, pp. 321–342.

[67] Farassat, F., and Succi, G. P., "A review of propeller discrete frequency noise prediction technology with emphasis on two current methods for time domain calculations," *Journal of Sound and Vibration*, Vol. 71, No. 3, 1980, pp. 399–419.

[68] Brès, G., Pérot, F., and Freed, D., "Properties of the lattice Boltzmann method for acoustics," *15th AIAA/CEAS Aeroacoustics Conference (30th AIAA Aeroacoustics Conference)*, 2009, p. 3395.

[69] Casalino, D., "An advanced time approach for acoustic analogy predictions," *Journal of Sound and Vibration*, Vol. 261, No. 4, 2003, pp. 583–612.

[70] Rainbird, J. M., Bianchini, A., Balduzzi, F., Peiró, J., Graham, J. M. R., Ferrara, G., and Ferrari, L., "On the influence of virtual camber effect on airfoil polars for use in simulations of Darrieus wind turbines," *Energy Conversion and Management*, Vol. 106, 2015, pp. 373–384.

[71] Bianchini, A., Balduzzi, F., Rainbird, J. M., Peiro, J., Graham, J. M. R., Ferrara, G., and Ferrari, L., "An Experimental and Numerical Assessment of Airfoil Polars for Use in Darrieus Wind Turbines: Part 1—Flow Curvature Effects," *Turbo Expo: Power for Land, Sea, and Air*, Vol. 56802, American Society of Mechanical Engineers, 2015, p. V009T46A006.

[72] Drela, M., "XFOIL: An analysis and design system for low Reynolds number airfoils," *Low Reynolds number aerodynamics*, Springer, 1989, pp. 1–12.

[73] Montgomerie, B., "Methods for root effects, tip effects and extending the angle of attack range to±180, with application to aerodynamics for blades on wind turbines and propellers," *FOI, Swedish Defence Research Agency, Stockholm, Sweden, Report No. FOI*, 2004.

[74] Shubham, S., Ianakiev, A., and Wright, N., "Review of standalone small-scale Darrieus wind turbines - a Nottingham case study," *17th EAWE PhD Seminar on Wind Energy*, 2021.

[75] Rezaeiha, A., Kalkman, I., and Blocken, B., "CFD simulation of a vertical axis wind turbine operating at a moderate tip speed ratio: Guidelines for minimum domain size and azimuthal increment," *Renewable energy*, Vol. 107, 2017, pp. 373–385.

[76] Shubham, S., Wright, N., and Ianakiev, A., "Application of Richardson extrapolation method to aerodynamic and aeroacoustic characteristics of low Reynolds number vertical axis wind turbines," *28th AIAA/CEAS Aeroacoustics 2022 Conference*, 2022, p. 3022.

[77] Meana-Fernández, A., Fernandez Oro, J. M., Argüelles Díaz, K. M., Galdo-Vega, M., and Velarde-Suárez, S., "Application of Richardson extrapolation method to the CFD simulation of vertical-axis wind turbines and analysis of the flow field," *Engineering Applications of Computational Fluid Mechanics*, Vol. 13, No. 1, 2019, pp. 359–376.

[78] Vassberg, J., "Challenges and accomplishments of the AIAA CFD drag prediction workshop series," *AVT-246 Specialists' Meeting on Progress and Challenges in Validation Testing for Computational Fluid Dynamics, Avila, Spain, Sept*, 2016, pp. 26–28.

[79] Pearson, C., "Vertical axis wind turbine acoustics," Ph.D. thesis, University of Cambridge, 2014.

[80] Paraschivoiu, I., *Wind turbine design: with emphasis on Darrieus concept*, Presses inter Polytechnique, 2002.

[81] Sheldahl, R. E., and Klimas, P. C., "Aerodynamic characteristics of seven symmetrical airfoil sections through 180-degree angle of attack for use in aerodynamic analysis of vertical axis wind turbines," Tech. rep., Sandia National Labs., Albuquerque, NM (USA), 1981.

[82] Avallone, F., Ragni, D., and Casalino, D., "On the effect of the tip-clearance ratio on the aeroacoustics of a diffuser-augmented wind turbine," *Renewable Energy*, Vol. 152, 2020, pp. 1317–1327.

[83] Lignarolo, L., Ragni, D., Scarano, F., Ferreira, C. S., and Van Bussel, G., "Tip-vortex instability and turbulent mixing in wind-turbine wakes," *Journal of Fluid Mechanics*, Vol. 781, 2015, pp. 467–493.

[84] De Tavernier, D., "Aerodynamic advances in vertical-axis wind turbines," 2021.

[85] Glegg, S., and Devenport, W., *Aeroacoustics of low Mach number flows: fundamentals, analysis, and measurement*, Academic Press, 2017.

[86] Botha, J., Rasam, A., Catháin, D., Rice, H., and Shahrokhi, A., "Some noise predictions for small wind turbines," *Proceedings of ISMA*, 2016, pp. 4019–4032.

[87] Botha, J., "Predictions of Rotor Broadband Noise," Ph.D. thesis, Trinity College Dublin. School of Engineering. Discipline of Mechanical . . . , 2018.